Dayside nitrogen and carbon escape on Titan: the role of exothermic chemistry

H. Gu, J. Cui, P. Lavvas, D.-D. Niu, X.-S. Wu, J.-H. Guo, F. He, Y. Wei

Dayside nitrogen and carbon escape on Titan: the role of exothermic chemistry

Article *in* Astronomy and Astrophysics · November 2019

DOI: 10.1051/0004-6361/201936826

8 authors, including:

Gu Hao
Sun Yat-Sen University
11 PUBLICATIONS **20** CITATIONS
SEE PROFILE

Jun Cui
Sun Yat-Sen University
53 PUBLICATIONS **162** CITATIONS
SEE PROFILE

Fei He
Institute of Geology and Geophysics Chinese Academy of Sciences
54 PUBLICATIONS **289** CITATIONS
SEE PROFILE

Astronomy & Astrophysics manuscript no. Chemical_escape_clean ©ESO 2019
October 23, 2019

Dayside nitrogen and carbon escape on Titan: The role of exothermic chemistry

H. Gu[1], J. Cui[2,3,4], P. P. Lavvas[5], D. -D. Niu[1], X. -S. Wu[3,4], J.-H. Guo[6], F. He[7], and Y. Wei[7]

[1] Space Science Institute, Macau University of Science and Technology, Macau, People's Republic of China
[2] School of Atmospheric Sciences, Sun Yat-Sen University, Zhuhai, Guangdong, People's Republic of China
[3] National Astronomical Observatories, Chinese Academy of Sciences, Beijing, People's Republic of China
[4] Chinese Academy of Sciences Center for Excellence in Comparative Planetology, Hefei, Anhui, People's Republic of China
[5] Université de Reims Champagne Ardenne, CNRS, GSMA UMR 7331, 51097 Reims, France
[6] Yunnan Astronomical Observatory, Chinese Academy of Sciences, Kunming, Yunnan, People's Republic of China
[7] Institute of Geology and Geophysics, Chinese Academy of Sciences, Beijing, People's Republic of China

October 23, 2019

ABSTRACT

Context. Atmospheric escape has an appreciable impact on the long-term climate evolution on terrestrial planets. Exothermic chemistry serves as an important mechanism driving atmospheric escape, and the role of such a mechanism is of great interest for Titan due to its extremely complicated atmospheric and ionospheric composition.

Aims. This study is devoted to a detailed investigation of neutral N and C escape on the dayside of Titan driven by exothermic neutral-neutral, ion-neutral, and dissociative recombination (DR) reactions, with the aid of the extensive measurements of Titan's upper atmospheric structure made by a number of instruments onboard Cassini, along with the improved understandings of the chemical network involved.

Methods. A total number of 14 C- and N-containing species are investigated based on 146 exothermic chemical reactions that release hot neutrals with nascent energies above their respective local escape energies. For each species and each chemical channel,

the hot neutral production rate profile is calculated, which provides an estimate of the corresponding escape rate when combined with the appropriate escape probability profile obtained from a test particle Monte Carlo model.

Results. Our calculations suggest a total N escape rate of 9.0×10^{23} s^{-1} and a total C escape rate of 4.2×10^{23} s^{-1} driven by exothermic chemistry and appropriate for the dayside of Titan. The former is primarily contributed by neutral-neutral reactions whereas the latter is dominated by ion-neutral reactions but the contributions from neutral-neutral and DR reactions cannot be ignored as well. Our calculations further reveal that the bulk of N escape occurs via hot N(^{4}S) production from the collisional quenching of N(^{2}D) by ambient N_2, and C escape is mainly driven by hot CH_3 and CH_4 production via a number of important ion-neutral and neutral-neutral reactions.

Conclusions. When compared with previous investigations of other known escape mechanisms, we suggest that exothermic chemistry plays an insignificant role in N escape but likely contributes appreciably to non-thermal C escape on the dayside of Titan.

Key words. planets and satellites: atmospheres – planets and satellites: individual (Titan)

1. Introduction

Solar Extreme Ultraviolet (EUV) and X-ray photons deposit a substantial amount of energy in a dayside planetary upper atmosphere, causing dissociation and ionization of ambient neutrals and initializing a complicated chemical network including neutral-neutral, ion-neutral, and dissociative recombination (DR) reactions (e.g. Fox et al. 2008). The chemical products from these reactions may gain sufficient energy and escape to the interplanetary space (e.g. Johnson et al. 2008).

Titan, the largest satellite of Saturn, has a thick and permanent atmosphere composed of N_2, CH_4, and H_2, along with various hydrocarbons, nitriles, and oxides as trace species (e.g. Waite et al. 2005; Niemann et al. 2005). Considerable neutral escape is thought to occur on Titan (e.g. Strobel, & Cui 2014). For neutral escape driven by exothermic chemistry, Cravens et al. (1997) predicted pre-Cassini escape rates of 2.5×10^{25} s^{-1} for total N and 4×10^{25} s^{-1} for total C, whereas De La Haye et al. (2007) estimated the post-Cassini escape rates to be 8.3×10^{24} s^{-1} and 7.2×10^{24} s^{-1}, respectively. In both studies, the ideal exobase approximation (e.g. Levine et al. 1978; Wallis 1978) was adopted to calculate the escape rates.

Other non-thermal or thermal escape mechanisms have also been explored on Titan (e.g. Johnson et al. 2008; Jiang et al. 2017). Shematovich et al. (2003) obtained a total N escape rate of 9.2×10^{24} s^{-1} due to N_2 dissociation by solar EUV/X-ray photons as well as photoelectrons. Atmospheric sputtering was estimated to cause a total N escape rate of $10^{24} - 10^{25}$ s^{-1} (Lammer & Bauer 1993; Shematovich et al. 2001, 2003; Michael et al.

2005) and a total C escape rate an order of magnitude lower (Gu et al. 2019). While the thermal evaporation of N-containing species is negligible on Titan, the same process likely drives strong C escape at a rate of $\sim 10^{27}$ s^{-1} in the form of slow hydrodynamic escape of CH_4 (e.g. Yelle et al. 2008; Strobel 2009; Cui et al. 2012; Strobel 2012a,b), despite that such a conclusion is still under debate (e.g. Tucker & Johnson 2009; Bell et al. 2010, 2011; Schaufelberger et al. 2012).

With the accumulation of extensive measurements of Titan's atmospheric neutral and ion densities (e.g. Cui et al. 2009a,b; Magee et al. 2009; Mandt et al. 2012), along with the improved understandings of Titan's atmospheric and ionospheric chemistry (e.g. Wilson, & Atreya 2004; Vuitton et al. 2006a,b, 2007, 2008; Lavvas et al 2008a,b; Krasnopolsky 2014; Vuitton et al. 2019), it is now timely to perform a state-of-the-art evaluation of neutral escape on this interesting body as driven by exothermic chemistry. We calculate in Sections 2 and 3 the production rates of relevant hot neutrals and their escape probabilities. The escape rates are then determined in Section 4 where we also discuss the relative contributions of various chemical channels. Finally, we discuss our results and end with concluding remarks in Section 5. If not stated explicitly, hot neutral species mentioned throughout the remaining of the paper always refer to those with nascent kinetic energies above the respective local escape energies.

2. Hot neutral production rates

Due to the relatively low gravity on Titan compared to other terrestrial planets, a large number of neutral species could gain sufficient kinetic energy from exothermic chemistry and escape. Here we consider 14 N- and C-containing species including N(^{4}S), N(^{2}D), $^3CH_2$, CH_3, NH, CH_4, NH_3, C_2H_2, C_2H_3, HCN, C_2H_4, N_2, C_2H_5, and C_2H_6 in the order of increasing molecular mass up to 30 Da. The respective range of escape energy is from 0.32 eV for N(^{4}S), N(^{2}D), and $^3CH_2$ to 0.68 eV for C_2H_6, all refereed to the exobase at an altitude of about 1500 km (Westlake et al. 2011; Cui et al. 2011). Other species lighter than 30 Da and all species heavier than 30 Da are not considered in the present investigation, either because their production rates are much lower or because they are more strongly bound by Titan's gravity.

In previous studies of neutral C and N escape driven by exothermic chemistry, the pre-Cassini investigation of Cravens et al. (1997) included CH, $^3CH_2$, CH_3, CH_4, C_2H, C_2H_2, C_2H_3, C_2H_4, C_3H_2, C_3H_3, C_4H_3, C_4H_4, C_5H_4, C_5H_5, N(^{4}S), N(^{2}D), NH, CN, HCN, and N_2, whereas the early post-Cassini investigation of De La Haye et al. (2007) included $^3CH_2$, CH_3, CH_4, C_2H_4, C_2H_5, C_2H_6, N(^{4}S), NH, N_2, and HCN. All species considered by De La Haye et al. (2007) have been properly included in the present study as well. When compared to Cravens et al. (1997), 9 species including CH, C_2H, CN, and 6 additional species heavier than 30 Da are not considered here because their contributions to total C

or N escape are negligible. The H and H_2 escape rates due to exothermic chemistry were also evaluated by De La Haye et al. (2007), but these escape rates are far less than the thermal evaporation rates (e.g. Cui et al. 2008; Hedelt et al. 2010; Strobel 2010).

The calculations of the hot neutral production rates are based on the combined list of exothermic chemical reactions presented in the literature (Cravens et al. 1997; De La Haye et al. 2007; Lavvas et al 2008a,b; Vuitton et al. 2007, 2019). For each reaction, the kinetic energy release is evaluated from the enthalpy difference at room temperature between the reactants and products both assumed to be in their ground states (Baulch et al. 2005). The energy partition between different products is taken to be inversely proportional to the molecular mass. Here we consider a subset of these reactions that produce candidate hot neutrals with kinetic energies exceeding the respective escape energies, as listed in Table A1 including 80 neutral-neutral reactions (of which 15 are three-body reactions), 31 ion-neutral reactions, and 35 DR reactions. The atmospheric and ionospheric chemical network implemented here is far more complicated and detailed than those adopted in Cravens et al. (1997) and De La Haye et al. (2007).

For both neutral-neutral and ion-neutral reactions, rate coefficients appropriate for a fixed temperature of 150 K are adopted (e.g. Snowden et al. 2013). The rate coefficient for a three-body reaction, k_3, is expressed as

$$k_3 = \frac{k_\infty(k_0[\mathrm{M}]X + k_R)}{k_\infty + k_0[\mathrm{M}]X}, \tag{1}$$

where [M] is the density of the background neutral species assumed to be exclusively N_2, k_0 and k_∞ are the termolecular and bimolecular rate constants, k_R is an additional rate constant introduced to include radiative association (Vuitton et al. 2012), the non-dimensional parameter, X, is given by $X = F/(1-F)$ with F defined as

$$\log F = \frac{\log(F_C)}{1 + [\frac{\log[P_r]+C}{N-0.14(\log[P_r]+C)}]^2}.$$

In the above expression, $P_r = k_0[\mathrm{M}]/k_\infty$, $N = 0.75-1.27\log F_C$, and $C = -0.4-0.67\log F_C$ with F_C being a fixed parameter for a specific reaction. For several three-body reactions with no available information on radiative association (R_d1, R_k1, and R_m1 in Table A1), the conventional Lindemann-Hinshelwood expression is used with $k_R = 0$ and $X = 1$ in Equation 1 (e.g. Hörst et al. 2008). A further exception is the three-body reaction R_k2 in Table A1 for which a constant value of $k_3[\mathrm{M}] \approx 2\times10^{-15}$ cm^3 s^{-1} is used following Lavvas et al (2008a) independent of altitude. The kinetic energy release for a three-body reaction is obtained in the same way as a two-body reaction, with the contribution from radiative association ignored for simplicity (Vuitton et al. 2012). Such an approximation should not lead to significant uncertainty in the derived escape fluxes since three-body reactions are overall unimportant in hot N and C production near and above the exobase (see below for

details). Finally, as normal the DR rate coefficient is assumed to be inversely proportional to a certain power of the electron temperature (e.g. Viggiano et al. 2005), with the power index in the range of 0.39−1.2 (see Table A1).

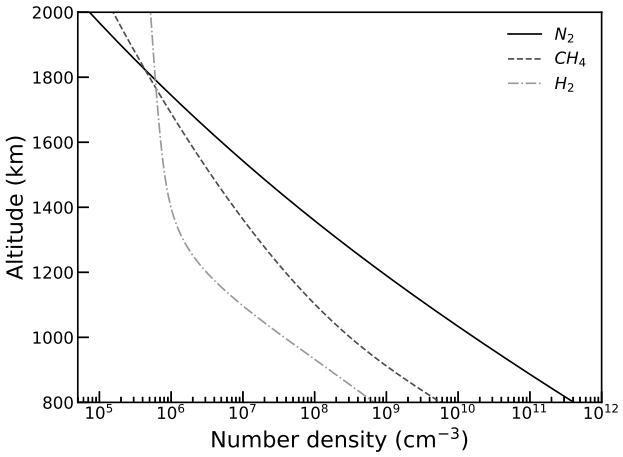

Fig. 1. The background neutral atmosphere of Titan for the 3 most abundant species, N_2, CH_4, and H_2, over the altitude range of 800−2000 km based on the dayside averaged Cassini INMS measurements in the CSN mode (Waite et al. 2005).

The background neutral atmosphere of Titan is displayed in Figure 1 for the 3 most abundant species, N_2, CH_4, and H_2, over the altitude range of 800−2000 km based on the dayside averaged Cassini Ion Neutral Mass Spectrometer (INMS) measurements in the closed source neutral (CSN) mode (Waite et al. 2005). All dayside INMS CSN data accumulated during 30 Cassini flybys with Titan, from TA on 26 October 2004 to T107 on 10 December 2014, are included and the neutral densities are extracted following the procedure described in Cui et al. (2008, 2012). The outbound density data are excluded to avoid possible contamination by the INMS wall effects (Cui et al. 2009a). The mixing ratio profiles for various neutral reactants necessary for determining the hot neutral production rates are displayed in Figure 2, adapted from the model results of Lavvas et al (2008a,b) up to an altitude of 1300 km. These profiles have been updated with the improved chemical network in Titan's atmosphere and ionosphere, and found to be in reasonable agreement with the latest Cassini INMS measurements. The species displayed in Figure 2 include 9 hydrocarbons (C_2H_2, C_2H_4, C_2H_6, C_3H_2, CH_3CCH, CH_2CCH_2, C_3H_6, C_3H_8, C_4H_{10}) in panel (a), 8 nitriles (NH_3, HCN, CH_2NH, CH_3CN, C_2H_3CN, C_2H_5CN, HC_3N, HC_5N) in panel (b), and 25 radicals (H, C, CH, $^3CH_2$, $^1CH_2$, CH_3, C_2, C_2H, C_2H_3, C_2H_5, C_3H_3, C_3H_5, C_3H_7, C_4H, C_4H_3, C_4H_5, C_4H_9, C_6H, C_6H_5, CN, C_2N, $N(^4S)$, $N(^2D)$, NH, NH_2) in panels (c) and (d), respectively. The mixing ratio profiles displayed in the figure are extrapolated to higher altitudes assuming diffusive equilibrium. Unlike ions (see below), the densities of most neutral reactants involved here are not directly measured by the INMS instrument (especially radicals), and accordingly we choose to use directly the model results.

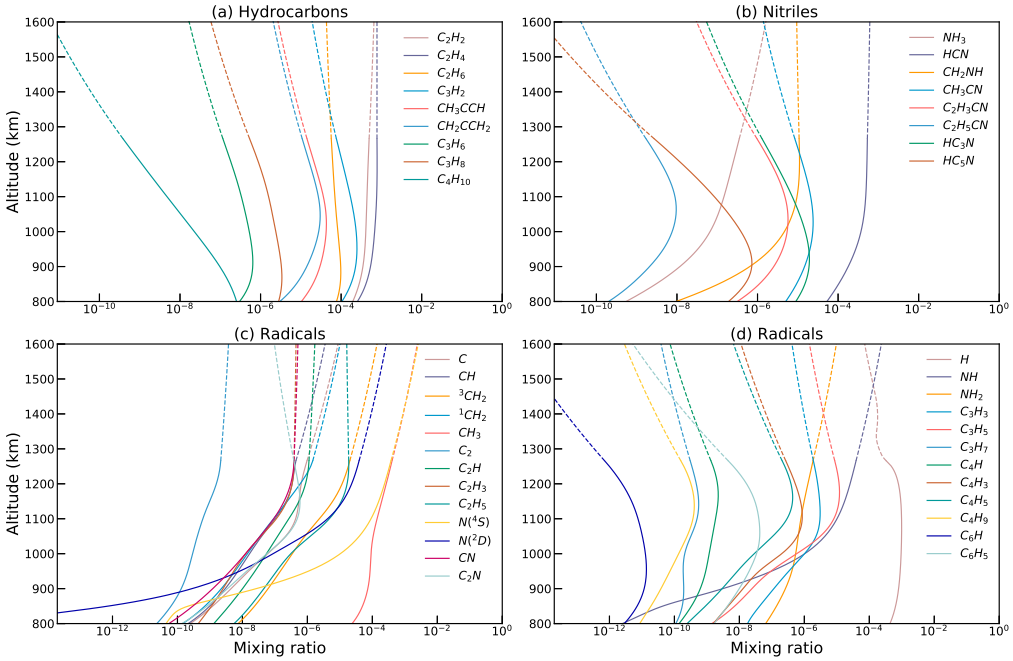

Fig. 2. The mixing ratio profiles of various neutral species in Titan's dayside upper atmosphere including hydrocarbons (a), nitriles (b), and radicals (c and d), adapted from the model results of Lavvas et al (2008a,b) at 800−1300 km which have been updated with the improved chemical network in Titan's atmosphere and ionosphere. These mixing ratio profiles are extrapolated to higher altitudes assuming diffusive equilibrium (indicated by the dashed lines).

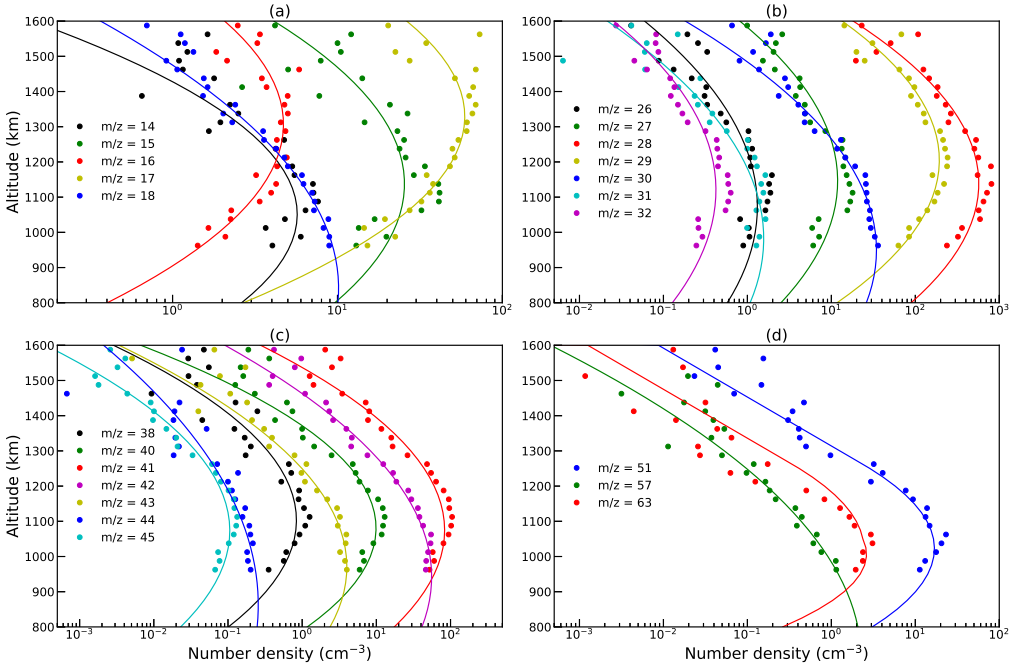

Fig. 3. The density profiles of ion reactants involved in this study, based on the Cassini INMS measurements in the OSI mode (solid circles) according to the mass-to-charge ratio, M/Z (Mandt et al. 2012). Also shown are the smooth empirical profiles based on the third-order polynomial fittings to logarithmic density (solid lines).

The density profiles of ion reactants used in this study are shown in Figure 3, extracted from the Cassini INMS measurements in the open source ion (OSI) mode (Mandt et al. 2012) according to the mass-to-charge ratio, M/Z. All dayside INMS OSI data from TA

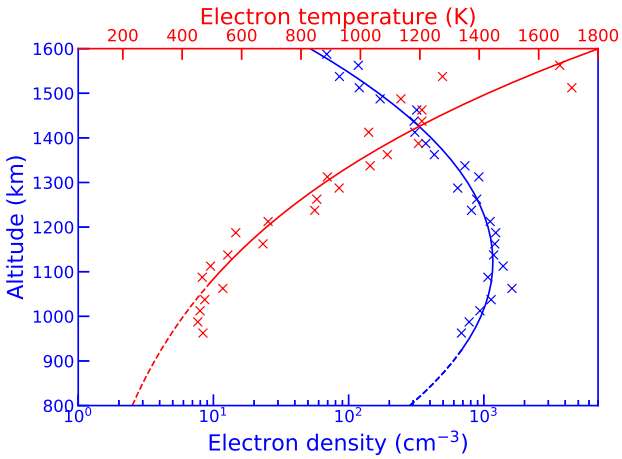

Fig. 4. The electron density and temperature profiles based on the Cassini RPWS LP measurements (crosses) averaged over the dayside of Titan (Wahlund et al. 2005). The empirical electron density profile (solid blue) is obtained in a similar manner as the ion density profiles in Figure 3, whereas the empirical electron temperature profile (solid red) is obtained by using the functional form of Ergun et al. (2015).

to T107 are included. The identification of the ion species follows the scheme of Vuitton et al. (2007): M/Z = 14 for N^+, 15 for CH_3^+, 16 for CH_4^+, 17 for CH_5^+, 18 for NH_4^+, 26 for CN^+, 27 for $C_2H_3^+$ and HCN^+, 28 for $C_2H_4^+$, N_2^+, and $HCNH^+$, 29 for $C_2H_5^+$ and N_2H^+, 30 for $C_2H_6^+$, 31 for $C_2H_7^+$, 32 for $CH_3NH_3^+$, 38 for CNC^+, 40 for $C_3H_4^+$, 41 for $C_3H_5^+$, 42 for $C_3H_6^+$, 43 for $C_3H_7^+$, 44 for $C_3H_8^+$, 45 for $C_3H_9^+$, 51 for $C_4H_3^+$, 57 for $C_4H_9^+$, and 63 for $C_5H_3^+$, respectively, all in unit of Da. For those channels sampling more than one ion species, the percentage contributions as a function of altitude are taken from Vuitton et al. (2019). For each species in Figure 3, the raw INMS measurements (solid circles) show considerable variability, and a smooth empirical profile (solid line) based on the third-order polynomial fitting to logarithmic density is used instead.

The electron density and temperature profiles, as displayed in Figure 4, are based on the Cassini Radio and Plasma Wave Science (RPWS) Langmuir Probe (LP) measurements made over the dayside of Titan (Wahlund et al. 2005). Note that the electron density is not necessarily identical to the total ion density due to the presence of positive ions heavier than 100 Da not sampled by the INMS and also due to the presence of negative ions (e.g. Wahlund et al. 2009). In Figure 4, the empirical electron density profile is obtained in a similar manner as the ion density profiles, whereas the empirical electron temperature profile is obtained by using the functional form of Ergun et al. (2015).

The total hot neutral production rates are calculated via the neutral, ion, and electron density profiles in Figures 1-4 and are displayed in Figures 5 and 6 for the 14 candidate escaping species quoted above. The contributions from all the 146 independent chemical channels listed in Table A1 are shown separately in Figures A1 and A2, where for clarification, the neutral-neutral, ion-neutral, and DR reactions are indicated by the solid, dashed, and dash-dotted lines, respectively. For each species, we identify the dominant produc-

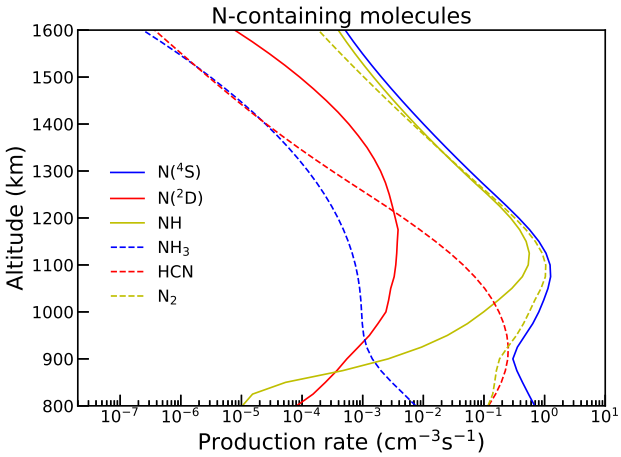

Fig. 5. The total hot neutral production rates for all the N-containing species considered in this study.

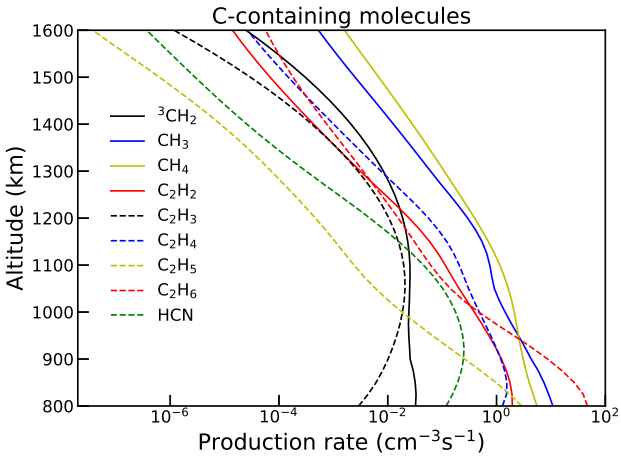

Fig. 6. Similar to Figure 5 but for all the C-containing species considered in this study.

tion channels, which are addressed in detail below. Whenever possible, we compare our results to those of De La Haye et al. (2007) in terms of the relative importances of different channels in hot neutral production.

N(^{4}S) and N(^{2}D): The chemical production of hot N in the form of ground state N(^{4}S) mainly occurs via the neutral-neutral reactions

$$\begin{aligned} &\mathrm{N}(^2\mathrm{D}) + \mathrm{N}_2 \rightarrow \mathrm{N}(^4\mathrm{S}) + \mathrm{N}_2 \quad (\mathrm{R}_a1), \\ &\mathrm{NH} + \mathrm{CH}_3 \rightarrow \mathrm{N}(^4\mathrm{S}) + \mathrm{CH}_4 \quad (\mathrm{R}_a2), \end{aligned} \tag{2}$$

followed by the ion-neutral reaction

$$\mathrm{N}^+ + \mathrm{CH}_4 \rightarrow \mathrm{N}(^4\mathrm{S}) + \mathrm{CH}_4^+ \quad (\mathrm{R}_a3), \tag{3}$$

of which R_a1 and R_a2 dominate above 950 km whereas R_a3 dominates at lower altitudes. R_a1 essentially represents the collisional quenching of N(^{2}D) to ground state N(^{4}S). The production of hot N in the form of excited state N(^{2}D) is of minor importance, mainly via

two DR reactions

$$\begin{aligned} N_2^+ + e &\rightarrow N(^4S) + N(^2D) \quad (R_a5), \\ N_2^+ + e &\rightarrow 2\ N(^2D) \quad (R_a6), \end{aligned} \tag{4}$$

which have comparable reaction rates at all altitudes of interest here.

NH and NH_3: The dominant channels of hot NH production are two neutral-neutral reactions

$$\begin{aligned} N(^4S) + C_2H_5 &\rightarrow NH + C_2H_4 \quad (R_c3), \\ N(^2D) + NH_3 &\rightarrow NH + NH_2 \quad (R_c4). \end{aligned} \tag{5}$$

The production rate of hot NH_3 is substantially lower, mainly contributed by the DR reaction

$$CH_3NH_3^+ + e \rightarrow NH_3 + CH_3 \quad (R_f2), \tag{6}$$

with a production rate at the exobase nearly 3 orders of magnitude smaller than the hot NH production rate at the same altitude. Note that R_f2 and R_c3 also produce hot CH_3 and C_2H_4 in Titan's upper atmosphere (see below). R_c6 in Table A1 does not contribute to NH_3 escape because the respective kinetic energy of 0.34 eV is below the NH_3 escape energy of 0.39 eV near Titan's exobase.

HCN: HCN is an effective coolant of Titan's upper atmosphere (Yelle 1991) and its abundance was recently obtained by Cui et al. (2016) at 1000−1400 km based on the Cassini INMS measurements in the CSN mode. For hot HCN production, the most important channel below 1400 km is the ion-neutral reaction

$$HCNH^+ + C_3H_3N \rightarrow HCN + C_3H_4N^+ \quad (R_h9), \tag{7}$$

which is due to the relatively high abundance of $HCNH^+$ in Titan's ionosphere (Cravens et al. 2005). Above 1400 km, hot HCN production is mainly contributed by the charge exchange reaction

$$HCN^+ + C_2H_2 \rightarrow HCN + C_2H_2^+ \quad (R_h7). \tag{8}$$

We also note that the ion-neutral reaction

$$CH_3^+ + HC_3N \rightarrow HCN + c\text{-}C_3H_3^+ \quad (R_h5), \tag{9}$$

is likely the most important channel producing hot HCN below 800 km but this reaction should not contribute to HCN escape as the escape probability at such low altitudes is

vanishingly small (see Section 3). De La Haye et al. (2007) identified the DR reaction

$$HCNH^+ + e \rightarrow HCN + H, \quad (10)$$

and the neutral-neutral reaction

$$H_2CN + H \rightarrow HCN + H_2, \quad (11)$$

194 to be most important in hot HCN production above and below 1070 km, respectively,
195 but these two reactions do not drive HCN escape since the corresponding nascent kinetic
196 energies are below the local escape energy.

N_2: The dominant channel for hot N_2 production is the collisional quenching reaction R_j2 (or R_a1 quoted above). Such a reaction is seriously reduced below 900 km and a number of ion-neutral reactions become more important with

$$\begin{aligned} N^+ + HCN &\rightarrow N_2 + CH^+ \quad (R_j3), \\ N_2^+ + C_2H_2 &\rightarrow N_2 + C_2H_2^+ \quad (R_j4), \end{aligned} \quad (12)$$

providing the highest hot N_2 production rates near the lower boundary. The importance of R_j2 (or R_a1) was also reported by De La Haye et al. (2007). However, those authors identified the ion-neutral reaction

$$N_2H^+ + CH_4 \rightarrow CH_5^+ + N_2, \quad (13)$$

to be more important above 1250 km while such a reaction is not considered here because the associated N_2 products have insufficiently energies to escape. Meanwhile, De La Haye et al. (2007) identified the collisional quenching reaction

$$^1CH_2 + N_2 \rightarrow {}^3CH_2 + N_2, \quad (14)$$

197 to be dominant near and below 1000 km but similarly, the kinetic energy release of this
198 reaction is too low to drive N_2 escape on Titan.

$^3CH_2$: Two reactions make the most important contributions to hot $^3CH_2$ production, with the DR reaction

$$C_2H_5^+ + e \rightarrow {}^3CH_2 + CH_3 \quad (R_b5), \quad (15)$$

dominating above 970 km and the ion-neutral reaction

$$N^+ + C_2H_4 \rightarrow {}^3CH_2 + HCNH^+ \quad (R_b2), \quad (16)$$

dominating at lower altitudes, respectively. R_b5 is also an important channel for the chemical loss of $C_2H_5^+$, making roughly one third of its total chemical loss at a representative altitude of 1050 km (Vuitton et al. 2007).

CH_3: The production of hot CH_3 in Titan's dayside upper atmosphere is very complicated and contributed by a large number of reactions. Below 1100 km, the dominant channel is the ion-neutral reaction

$$N^+ + CH_4 \rightarrow CH_3 + NH^+ \quad (R_d24), \tag{17}$$

whereas at higher altitudes, two neutral-neutral reactions

$$\begin{aligned} N(^4S) + C_2H_5 &\rightarrow CH_3 + H_2CN \quad (R_d17), \\ N(^2D) + CH_4 &\rightarrow CH_3 + NH \quad (R_d19), \end{aligned} \tag{18}$$

one ion-neutral reaction

$$HCN^+ + CH_4 \rightarrow CH_3 + HCNH^+ \quad (R_d25), \tag{19}$$

and another DR reaction, which is R_b5 quoted above, become near equally important.

CH_4: Hot CH_4 production occurs mainly via the ion-neutral reaction

$$CH_5^+ + HCN \rightarrow CH_4 + HCNH^+ \quad (R_e13), \tag{20}$$

followed by 3 additional ion-neutral reactions

$$\begin{aligned} CH_5^+ + C_2H_2 &\rightarrow CH_4 + C_2H_3^+ \quad (R_e11), \\ CH_5^+ + C_2H_4 &\rightarrow CH_4 + C_2H_5^+ \quad (R_e12), \\ C_2H_5^+ + C_2H_4 &\rightarrow CH_4 + C_3H_5^+ \quad (R_e15), \end{aligned} \tag{21}$$

as well as the neutral-neutral reaction

$$CH_3 + NH \rightarrow CH_4 + N(^4S) \quad (R_e7), \tag{22}$$

of which the last one also contributes to hot $N(^4S)$ production near Titan's exobase. According to Vuitton et al. (2007), the former 4 reactions are important chemical loss channels of CH_5^+ and $C_2H_5^+$ in Titan's ionosphere. A similar reaction, R_e14 in Table A1, plays a minor role due to the relatively low rate coefficient (McEwan & Anicich 2007). For comparison, De La Haye et al. (2007) identified the DR reaction R_e17 to be dominant but this reaction is unimportant according to our calculations. The difference is partly due to the overestimate of the CH_5^+ abundance near Titan's exobase by De La Haye et al. (2007), essentially based on the pre-Cassini model results of Keller et al. (1992), and partly due to

the extremely high DR coefficient used by those authors, more than a factor of 10 higher than our value (see Table A1). For the 4 ion-neutral reactions listed in Equations 20 and 21, the relative contributions from reactions R_e12 and R_e15 comparable to our estimates were obtained by De La Haye et al. (2007) whereas reactions R_e11 and R_e13 were not considered by those authors. The neutral-neutral reaction R_e7 was also not included in their study.

C_2H_2: Hot C_2H_2 is mainly produced via the neutral-neutral reaction

$$CH_3 + C_2H_3 \rightarrow C_2H_2 + CH_4 \quad (R_g7), \tag{23}$$

above 1150 km and via another neutral-neutral reaction

$$C_2H + CH_2CCH_2 \rightarrow C_2H_2 + C_3H_3 \quad (R_g11), \tag{24}$$

at lower altitudes. R_g7 is also capable of driving CH_4 escape on Titan.

C_2H_3: The production of hot C_2H_3 is dominated by the DR reaction

$$C_3H_5^+ + e \rightarrow C_2H_3 + {}^3CH_2 \quad (R_i5), \tag{25}$$

at all altitudes of interest here, which is also the third most important channel for $^3CH_2$ production above 1100 km. In addition, the neutral-neutral reaction

$$C_2H_3CN + C_2 \rightarrow C_2H_3 + C_3N \quad (R_i3), \tag{26}$$

is an important channel producing hot C_2H_3 at low altitudes and does not contribute appreciably to C_2H_3 escape on Titan.

C_2H_4: Hot C_2H_4 production in Titan's dayside upper atmosphere is mainly driven by two neutral-neutral reactions

$$\begin{aligned} CH + C_2H_6 &\rightarrow C_2H_4 + CH_3 \quad (R_k3), \\ CH_3 + C_2H_5 &\rightarrow C_2H_4 + CH_4 \quad (R_k9), \end{aligned} \tag{27}$$

and two ion-neutral reactions

$$\begin{aligned} C_2H_5^+ + CH_3CN &\rightarrow C_2H_4 + CH_3CNH^+ \quad (R_k24), \\ C_2H_5^+ + HC_3N &\rightarrow C_2H_4 + HC_3NH^+ \quad (R_k25). \end{aligned} \tag{28}$$

The relative importances of different reactions vary with altitude, with R_k9 dominating above 1100 km, R_k24 at 960-1100 km, and R_k3 below 960 km, respectively. R_k3 and R_k9 also contribute to hot CH_3 and CH_4 production, though of minor importance only.

C_2H_5: The production of hot C_2H_5 occurs mainly via two DR reactions

$$\begin{aligned} &C_3H_6^+ + e \rightarrow C_2H_5 + CH \quad (R_l6), \\ &C_3H_8^+ + e \rightarrow C_2H_5 + CH_3 \quad (R_l7), \end{aligned} \tag{29}$$

and one neutral-neutral reaction

$$C_2H + C_2H_6 \rightarrow C_2H_5 + C_2H_2 \quad (R_l4). \tag{30}$$

However, hot C_2H_5 production below 930 km is dominated by the three-body reaction

$$H + C_2H_4 + M \rightarrow C_2H_5 + M \quad (R_l1). \tag{31}$$

Clearly, C_2H_5 escape on Titan is primarily driven by the former 3 reactions. Note also that R_l7 makes only a minor contribution to hot CH_3 production. Our calculations highlight the impact of radiative association on hot neutral production in the tenuous part of Titan's upper atmosphere. For instance, the conventional Lindemann-Hinshelwood formulism that does not include radiative association predicts a C_2H_5 production rate via Reaction R_l1 about 4 orders of magnitude too low near the exobase.

C_2H_6: Hot C_2H_6 production at all altitudes is dominated by the three-body reaction

$$2\ CH_3 + M \rightarrow C_2H_6 + M \quad (R_m2), \tag{32}$$

followed by the DR reaction

$$C_3H_7^+ + e \rightarrow C_2H_6 + CH \quad (R_m8). \tag{33}$$

In contrast, De La Haye et al. (2007) reported the latter reaction to be dominant at high altitudes as those authors did not include radiative association and therefore seriously underestimated hot C_2H_6 production near and above the exobase.

Finally, it is noteworthy that in most cases, three-body reactions are only important in the relatively dense regions of Titan's upper atmosphere where escape becomes difficult (see Section 3). Accordingly, their contributions to total N escape (in the form of N_2 recoils) is ignored in Table A1 and throughout this paper. An exception is reaction R_m2 which dominates C_2H_6 production at sufficiently high altitudes, but this reaction should not contribute substantially to N escape in the form of N_2 recoils because the respective production rate is well below the N_2 production rate via the collisional quenching reaction R_j2 (see above).

3. Hot neutral escape probabilities

For each species discussed in Section 2, the respective escape probability in Titan's dayside upper atmosphere is required to calculate rigorously the escape rate. The ideal exobase approximation was adopted by both Cravens et al. (1997) and De La Haye et al. (2007), essentially reflecting a sharp transition in escape probability from 0 to 0.5 at the exobase. Here to capture the realistic behavior of escaping neutrals over a broad transition region near the exobase, a more sophisticated test particle Monte Carlo model is constructed to obtain the escape probabilities of hot neutrals produced via each exothermic chemical channel. The model is analogous to previous models of atomic O escape on the dayside of Mars (e.g. Fox, & Hać 2009, 2014, 2018), and is modified from our existing model of atmospheric sputtering on Titan (Gu et al. 2019). We also mention that analytic models capable of capturing the near exobase transition of escape probability in an approximate manner have also been proposed such as the single collision model of Cravens et al. (2017) and the multiple collision model of Cui et al. (2019).

The plane parallel background atmosphere used in this study is displayed in Figure 1, over the altitude range of 800−2000 km and containing N_2, CH_4, and H_2. Below 800 km, the mean free path for collision is sufficiently short that the energy of a typical hot neutral is degraded rapidly to the local thermal energy over a length scale not exceeding 0.5 km, a situation consistent with local thermalization. At 2000 km, the collision probability drops to around 1%, implying that Titan's atmosphere above this altitude does not exert an appreciable influence on the derived escape probabilities. For the energy range encountered in this study, inelastic collision processes such as excitation and dissociation could be safely ignored. Similar to De La Haye et al. (2007), the collisions between hot neutrals and ambient neutrals are modeled under the hard sphere approximation for elastic collisions, with the appropriate hard sphere radii of relevant neutrals estimated from existing laboratory measurements of pure gas viscosity (e.g. Flynn & Thodos 1961; Fenghour et al. 1995; Rowley et al. 2003). Whenever no viscosity measurements have been made for a certain species, its hard sphere radius is either approximated by the known radius of a species in the same chemical group or taken from the American Chemical Society website on `http://center.acs.org/periodic/tools/PT.html`.

At a given altitude, a hot neutral particle is released in a random direction assuming isotropic production and with a prescribed nascent velocity depending on the chemical channel involved. The trajectory of this particle is followed under the influence of Titan's gravity and the position where it makes a further collision with ambient neutrals is determined in a stochastic manner with the aid of the known information of the collision cross section and the known structure of the background atmosphere. The collision partner, N_2, CH_4, or H_2, is also decided stochastically based on the column density ratio between different ambient species over the path length of hot neutral free propagation. The post-collision

velocities of both the hot neutral and the ambient neutral could then be favorably determined from the momentum and energy conservation laws, where the pre-collision velocity of the ambient neutral is assumed to be zero since its thermal energy (Snowden et al. 2013) and wind-driven bulk kinetic energy (Müller-Wodarg et al. 2008) are both well below the kinetic energy release from exothermic chemistry. The post-collision velocity direction of the hot neutral is also chosen randomly under the assumption of isotropic scattering. The above procedure is repeated until one of the following conditions is satisfied: (1) When the hot neutral reaches the lower boundary or when its kinetic energy falls below the local escape energy via a cascade of collisions anywhere within the simulation box, it is no longer traced in our model calculations; (2) When the hot neutral reaches the upper boundary, it is either assumed to be lost from the atmosphere or reflected downward elastically, depending on whether its kinetic energy is above or below the local escape energy.

The entire background atmosphere of Titan is divided into 17 altitude grids, each covering a depth of 50 km, to allow the full altitude profile of escape probability to be constructed. For each species, we consider a range of energy (see Table A2) that incorporates the range of nascent kinetic energy for various source reactions (see Section 2). For a unique combination of the nascent energy and the altitude of production, a total number of 100,000 hot neutrals are modeled independently to achieve statistically robust results for each species and each reaction.

In Figure 7, we show the escape probability as a function of altitude for each candidate escaping species quoted in Section 2 and for a sequence of nascent kinetic energy quoted in the figure legend. Several interesting features are immediately seen in the figure. First, all profiles reveal the presence of a broad transition region with a depth of nearly 200 km around the ideal exobase at 1500 km (Westlake et al. 2011). The escape probability is vanishingly small at the lower end of the transition region and is around 0.5 at the upper end. The latter is consistent with the expected scenario that nearly all particles moving upward are able to escape (e.g. Cravens et al. 1997). The actual escape probability at the upper end might be modestly different from the ideal value of 0.5 due to non-negligible backscattering. Second, the escape probability increases with increasing energy at all altitudes, which is interpreted by the fact that a more energetic particle allows a greater number of collisions before its energy falls below the local escape energy (e.g. Cui et al. 2019). Third, the escape probability also varies from species to species due to the difference in collision cross section. As intuitively expected, the escape probabilities of small hot particles tend to be higher than those of large hot particles as small ones are less likely to collide with ambient neutrals (e.g. Fox, & Hać 2014).

Despite the variations with both energy and collision cross section, we find that the modeled altitude profile of the escape probability, $\zeta_{\rm esc}$, could be reasonably described by a

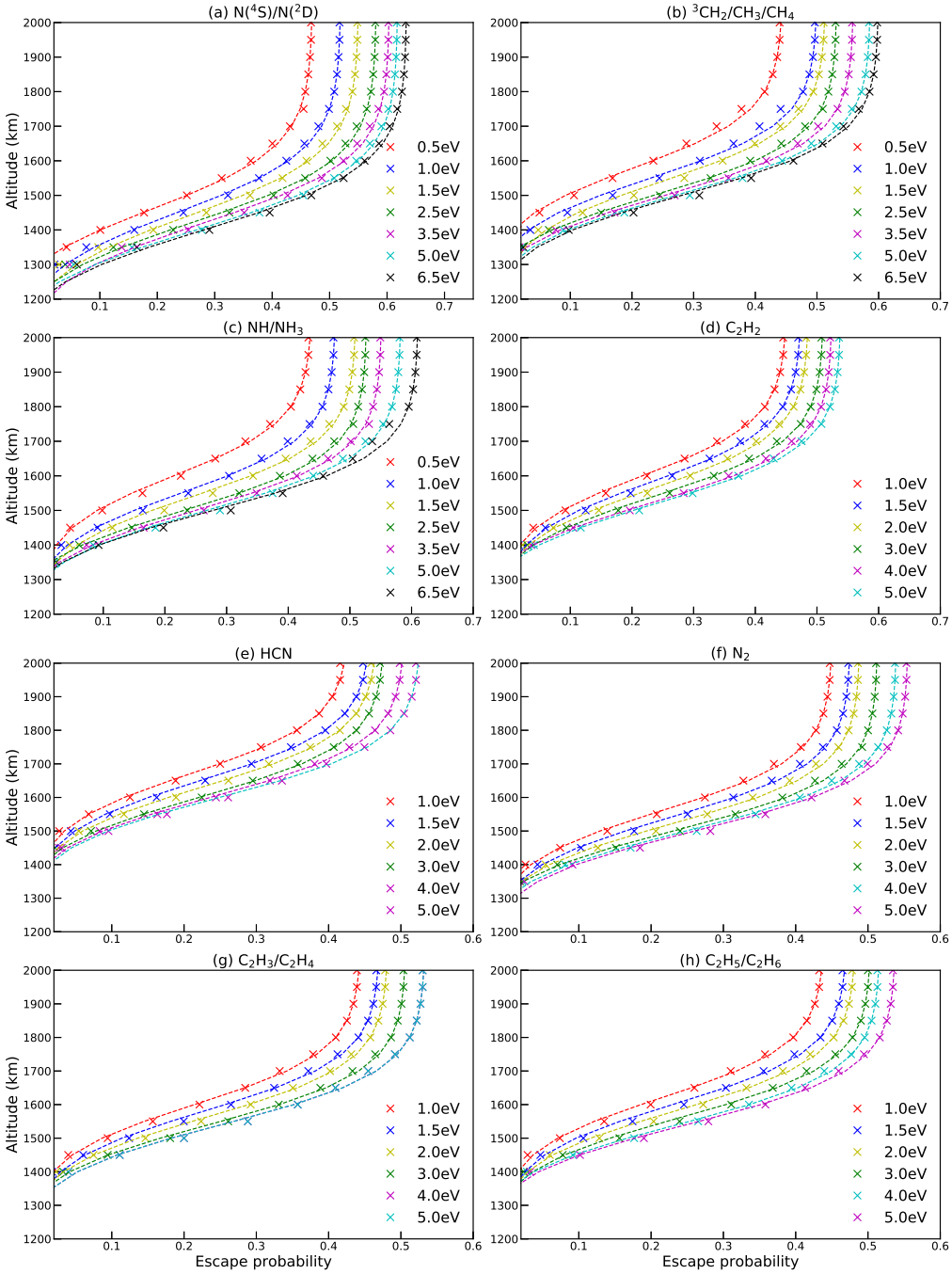

Fig. 7. Escape probability profiles for various hot neutrals and covering the range of nascent kinetic energy encountered in this study. The crosses are adapted from test particle Monte Carlo calculations whereas the dashed lines indicate the best empirical fits (see text for details).

common functional form of

$$\zeta_{\rm esc} = a_1 \tanh(\frac{z - a_2}{160}) + a_3, \tag{34}$$

where z is the altitude in km, a_1, a_2, and a_3 are free parameters to be constrained by the Monte Carlo model results. As motivated by Figure 7, we adopt a common depth of 160 km for the transition region for all species and at all nascent energies. In the equation, a_2 denotes the central location of the transition region, whereas $a_3 + a_1$ represents the

asymptotic escape probability at sufficiently high altitudes. Ideally, one may expect that the asymptotic escape probability at low altitudes, given by $a_3 - a_1$ according to Equation 34, should be zero, thus implying $a_1 = a_3$. However, such a condition does not always lead to satisfactory fits to the modeled escape probability profiles. Accordingly, Equation 34 cannot be extrapolated to arbitrarily low altitudes where the predicted escape probability could sometimes be negative. The best-fit profiles of escape probability are indicated by the dashed lines in Figure 7 for reference.

Since the location of the transition region appears to be energy independent according to Figure 7, we assume for simplicity a constant value of a_2 for any given species, as listed in Table A2. a_1 and a_3 are clearly energy dependent and described in this study by

$$\begin{aligned} a_1 &= b_1 \exp(-E) + b_2 \qquad (a), \\ a_1 &= b_1 \ln E + b_2 \qquad (b), \\ a_3 &= b_3 \ln E + b_4 \qquad (c), \end{aligned} \tag{35}$$

where E is the nascent energy of a hot particle in eV, b_1, b_2, b_3, and b_4 are free parameters to be constrained by the values listed in Table A2. Note that Equation 35a is used to describe the a_1 parameters of relatively light species including N(^{4}S), N(^{2}D), $^3CH_2$, CH_3, CH_4, NH, and NH_3, whereas Equation 35b is used for heavier species considered in this study. Combining Equations 34 and 35, we are able to obtain the escape probability profile for any candidate escaping species and at any nascent energy.

4. Neutral escape rates driven by exothermic chemistry

The escape rate for a given species and a given chemical channel in Titan's dayside upper atmosphere, as listed in Table A1, is estimated via

$$\Phi_{\rm esc} = \int_{800\ \rm km}^{1600\ \rm km} 2\pi (R_{\rm T} + z)^2 \zeta_{\rm esc}(z) P_{\rm hot}(z) dz, \tag{36}$$

where $R_{\rm T}$ is Titan's solid body radius, $P_{\rm hot}$ is the hot neutral production rate, and the other parameters are defined above. Combining the calculations for all the 14 species and all the 146 independent chemical channels, we are able to obtain the total C and N escape rates, as well as determine the relative contribution of each channel. For reference, we provide in Table A1 the escape rates of all neutral species via all chemical channels involved in this study, along with the respective fractional contributions to total C or N escape. We caution that a channel with a large column integrated hot neutral production rate does not necessarily contribute substantially to neutral escape since peak production may occur at low altitudes where the escape probability is small.

Table A1 reveals that for N escape, the most important channel is the collisional quenching reaction R_a1 which contributes to 80% of total N escape via exothermic chemistry, in

the form of both hot N(^{4}S) and hot N_2 (note that the N_2 escape rate listed in Table A1 for R_j2 is multiplied by 2 to represent the net N escape rate). The second most important channel is the neutral-neutral reaction R_a2 that produces hot N(^{4}S) and accounts for 12% of total N escape. Two other neutral-neutral reactions, R_c3 and R_c5, contribute non-negligibly to 8% of total N escape by producing hot NH. It is interesting to note that the contribution from hot NH production to total N escape is higher than the contribution from hot N_2 production. This is an unexpected result that was not reported by Cravens et al. (1997) and De La Haye et al. (2007) despite that both studies included NH-related chemistry. Ion-neutral and DR reactions are less important than neutral-neutral reactions in driving N escape. Specifically, the most important ion-neutral reaction is R_a3 and the most important DR reaction is R_a5, but they only contribute to 0.6% and 2.6% of total N escape by producing either hot N(^{4}S) or hot N(^{2}D).

Total C escape in Titan's dayside upper atmosphere driven by exothermic chemistry occurs in a more complicated manner, with 16 reactions making fractional contributions above 1% including 6 neutral-neutral, 7 ion-neutral and 3 DR reactions. The most important channel is the ion-neutral reaction R_e13 producing hot CH_4 and Table A1 indicates that this reaction contributes to about 30% of total C escape. The next two important channels are the neutral-neutral reactions R_e7 and R_e12 that also produce hot CH_4, each contributing to 9% of total C escape. In addition, several other channels of hot CH_3 and CH_4 production account for a non-negligible fraction of total C escape no less than 5%, mainly via 2 neutral-neutral reactions R_d17, R_d19, and 2 ion-neutral reactions R_d25 and R_e11. Reaction R_e7 is also the second most important channel driving total N escape (R_a2 quoted above) since this reaction produces both hot CH_4 and hot N(^{4}S). The contribution from DR reactions to total C escape is less important, mainly via R_b5 (which is also R_d29 in Table A1) producing both hot $^3CH_2$ and hot CH_3, and via R_e19 producing hot CH_4.

The C and N escape rates due to the production of different hot neutral species are compared schematically in Figure 8, with the contributions from neutral-neutral, ion-neutral, and DR reactions indicated separately. The total dayside N escape rate is 9.1×10^{23} s^{-1} with more than 95% from neutral-neutral reactions and the remaining fraction partitioned between ion-neutral and DR reactions. The total dayside C escape rate is 4.3×10^{23} s^{-1} with 60% from ion-neutral reactions, 29% from neutral-neutral reactions, and the remaining 11% from DR reactions, respectively. Our calculations indicate that about 86% of total N escape is contributed by hot N(^{4}S) and N(^{2}D) production, followed by nearly 8% from hot NH production and 6% from hot N_2 production. Note that ion-neutral reactions do not contribute to NH escape and DR reactions do not contribute to N_2 escape according to Figure 8. Total C escape is partitioned mostly among three species: 63% from CH_4 escape, 27% from CH_3 escape, and 4% from $^3CH_2$ escape. The combined fractional contribution from the remaining C-containing species is only 6%.

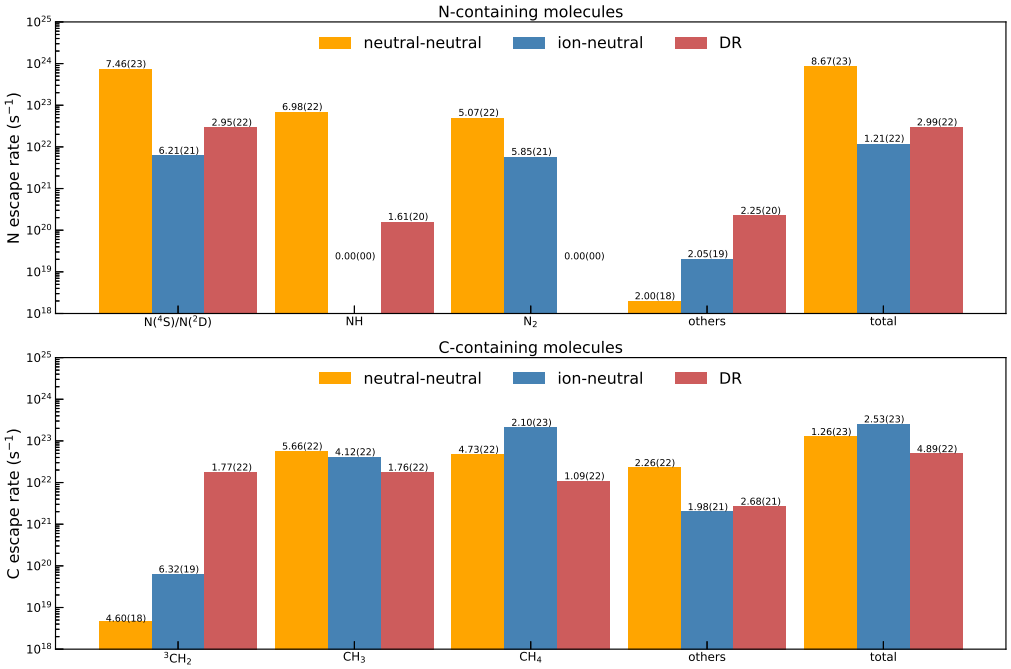

Fig. 8. The C and N escape rates via the production of different N- and C-containing species, with the contributions from neutral-neutral, ion-neutral, and DR reactions indicated separately.

For all the three categories of exothermic chemistry considered here, we find that neutral-neutral reactions drive N escape nearly a factor of 7 stronger than C escape, ion-neutral reactions drive C escape nearly a factor of 20 stronger than N escape, whereas DR reactions drive comparable C and N escape, respectively. We emphasize that to describe properly total N escape, both ion-neutral and DR reactions could be ignored with an uncertainty no more than 5%, whereas to describe properly total C escape, all categories of exothermic reaction have to be taken into account.

5. Discussions and concluding remarks

Atmospheric escape is a key process that controls the evolution of climate and habitability on terrestrial planets. One of the important mechanisms driving atmospheric escape is exothermic chemistry that may produce hot neutrals sufficiently energetic to overcome the gravitational potential of the central body (e.g. Johnson et al. 2008, and references therein). This mechanism is especially interesting for Titan, the largest satellite of Saturn, due to its extremely complicated atmospheric and ionospheric composition as revealed by the Cassini INMS measurements in both the CSN and OSI modes (e.g. Waite et al. 2005; Cravens et al. 2005). The total C and N escape rates on the dayside of Titan driven by exothermic chemistry were computed in the pre-Cassini investigation of Cravens et al. (1997) and the early post-Cassini investigation of De La Haye et al. (2007) (when the data from a very limited number of close Titan flybys were available). The present investigation is intended for an updated evaluation of the same issue by virtue of the extensive Cassini INMS measurements of Titan's upper atmospheric structure (e.g. Cui et al. 2009a,b; Magee

et al. 2009; Mandt et al. 2012) as well as the improved understandings of the associated chemical network over the past decade (e.g. Wilson, & Atreya 2004; Vuitton et al. 2006a,b, 2007, 2008; Lavvas et al 2008a,b; Krasnopolsky 2014; Vuitton et al. 2019).

A total number of 14 candidate escaping neutral species are considered in this study including $N(^4S)$, $N(^2D)$, $^3CH_2$, CH_3, NH, CH_4, NH_3, C_2H_2, C_2H_3, HCN, C_2H_4, N_2, C_2H_5, and C_2H_6 in the order of increasing molecular mass up to 30 Da. A total number of 146 exothermic chemical reactions are evaluated, all of which are capable of producing hot neutrals with nascent kinetic energies above the respective local escape energies. These reactions fall into three categories, including 80 neutral-neutral reactions (of which 15 are three-body reactions), 31 ion-neutral reactions, and 35 DR reactions. The atmospheric and ionospheric chemical network implemented here is far more complicated than those of Cravens et al. (1997) and De La Haye et al. (2007).

Combining the state-of-the-art INMS measurements of neutral and ion densities, the RPWS LP measurements of electron density and temperature, as well as the photochemical model results of Lavvas et al (2008a,b) updated with the improved chemical network, we are able to calculate the hot neutral production rate as a function of altitude for each species and each chemical channel in Titan's dayside upper atmosphere. A test particle Monte Carlo model is further constructed to determine the corresponding profile of escape probability under the assumption of isotropic hard sphere approximation, which properly describes the realistic dynamical behavior of escaping neutrals over a broad transition region near Titan's exobase (e.g. Strobel, & Cui 2014). Our model results are consistent with the intuitively expected trend that at any given altitude, the escape probability increases with the nascent kinetic energy and decreases with the size of the escaping particle. Calculations of the hot neutral production rate and the escape probability are combined to provide a reasonable estimate of the escape rate for each species and each channel.

Our calculations suggest a total N escape rate of 9.1×10^{23} s^{-1} and a total C escape rate of 4.3×10^{23} s^{-1} on the dayside of Titan, driven by exothermic chemistry. Total N escape is primarily contributed by neutral-neutral reactions, with a fractional contribution of less than 5% from ion-neutral and DR reactions. The situation for C escape is different in that all categories of reaction are non-negligible, with 60% from ion-neutral, 29% from neutral-neutral, and the remaining 11% from DR reactions, respectively. Meanwhile, the bulk of N escape is associated with hot $N(^4S)$ production and driven by the quenching of excited state $N(^2D)$ via collisions with atmospheric N_2. Such a process, denoted as R_a1 in Table A1, accounts for 80% of dayside N escape on Titan. Hot NH production also contributes non-negligibly to N escape and plays an even more important role than hot N_2 production, a result that was not obtained in previous investigations (Cravens et al. 1997; De La Haye et al. 2007). Dayside C escape is mostly associated with hot CH_3 and CH_4 production, responsible for 27% and 63% of total C escape, respectively. Our calculations

highlight the importance of one ion-neutral reaction: R_e13 that produces hot CH_4 from CH_5^+ and HCN, which accounts for more than 30% of dayside C escape on Titan. While the importance of reaction R_a1 in driving N escape was also obtained by De La Haye et al. (2007), the situation for C escape is to be distinguished in that those authors identified CH_5^+ DR as the most important chemical channel but we find it to be negligible. Such a difference is likely linked to the different choices of the DR coefficient and CH_5^+ density. It is noteworthy that the De La Haye et al. (2007) results were obtained based on the early photochemical model calculations of Keller et al. (1992) and our current understandings of Titan's atmospheric and ionospheric chemistry are much more robust (e.g. Vuitton et al. 2019).

It is instructive to compare the total dayside N and C escape rates driven by exothermic chemistry to those by other viable mechanisms, especially the non-thermal ones (Johnson et al. 2008). Specifically, N_2 photodissociation is ignored in this study but existing works indicate that this process likely leads to a dayside averaged N escape rate much higher than the value reported here. For instance, the calculations of Shematovich et al. (2003) suggest an N escape rate of 9×10^{24} s^{-1} driven by N_2 photodissociation, which is an order of magnitude higher than our estimate of the chemically driven N escape rate. Without showing the details, we mention that the photochemical model implemented in Section 3 leads to a comparable dayside N escape rate of 8×10^{24} s^{-1} via $N(^4S)$ production from N_2 photodissociation, where the escape probability profile appropriate for 0.82 eV is used based on the mean kinetic energy release to $N(^4S)$ weighted by the solar EUV/X-ray flux above the N_2 dissociation threshold, for a reference altitude of 1400 km. Photoelectron impact dissociation of N_2, which was evaluated by Cravens et al. (1997), may increase further the above N escape rate. Similarly, we estimate the dayside C escape rate to be 2×10^{24} s^{-1} via CH_3 production from CH_4 photodissociation, where a weighted mean kinetic energy of 0.46 eV is used to obtain the CH_3 escape probability profile. Clearly, C escape driven by exothermic chemistry is not negligibly small as compared to C escape driven by CH_4 photodissociation.

Atmospheric sputtering, as another viable escape mechanism, was modeled by a number of authors based on Monte Carlo calculations (e.g. Shematovich et al. 2001, 2003; Michael et al. 2005). The sputter-induced total N escape rate, contributed by both N and N_2, was predicted to be 4×10^{25} s^{-1} by the one-dimensional calculations of Shematovich et al. (2003) and 2.5×10^{25} s^{-1} by the three-dimensional calculations of Michael et al. (2005). Recently, Gu et al. (2019) estimated the CH_4-to-N_2 sputtering yield ratio in Titan's upper atmosphere to be 10%−20%, which should be close to the respective ratio in escape rate. When compared with the N and C escape rates derived here, we may conclude that sputter-induced N and C escape is much stronger than chemically driven escape. However, we note that the sputter-induced escape rates quoted above are appropriate for the ramside of Titan

which could be either the dayside or the nightside depending on the relative orientation between solar EUV/X-ray radiation and magnetospheric ion precipitation (Sittler et al. 2010, and references therein). This means that when Titan is in an orbital configuration with the dayside coincident with the wakeside, N and C escape driven by exothermic chemistry is likely much stronger than sputter-induced escape.

Clearly, all exothermic chemical reactions evaluated in this study, along with many other reactions ignored due to the non-escaping nature of their products, may provide an important heat source of Titan's upper atmosphere. For instance, the calculations of de La Haye et al. (2008) suggested that on both the dayside and nightside of the satellite, neutral heating via exothermic chemistry was dominated by ion-neutral and DR reactions above $\sim$ 1100 km, by two-body neutral-neutral reactions at $\sim 750 - 1100$ km, and by three-body neutral-neutral reactions at lower altitudes, respectively (see their Figure 10). These authors estimated a peak heating rate in Titan's dayside upper atmosphere of $\sim 5 \times 10^{-9}$ ergs cm^{-3} s^{-1} near 950 km driven by exothermic chemistry, well above the peak heating rate of no more than 10^{-10} ergs cm^{-3} s^{-1} near 1050 km driven by photoelectron and magnetospheric electron impact. Similarly, the DR reaction of O_2^+, the dominant species of the Venusian ionosphere (Taylor et al. 1980), was suggested to contribute significantly to dayside neutral heating, surpassing other important heating mechanisms such as the collisional quenching of excited state O(^{1}D) and the photodissociation of background CO_2 above 135 km (e.g. Fox 1988). Similar calculations as implemented here, also by virtue of the extensive Cassini INMS measurements of Titan's atmospheric neutral and ion densities (e.g. Cui et al. 2009a; Mandt et al. 2012), the improved understandings of Titan's atmospheric and ionospheric chemistry (e.g. Vuitton et al. 2019), as well as the realistic Monte Carlo modeling of energy deposition including transport (e.g. Michael, & Johnson 2005), should be able to reveal more rigorously the importance of various exothermic chemical reactions in the local energy budget of Titan's upper atmosphere, which we leave for follow-up investigations.

Acknowledgements. This work is supported by the Strategic Priority Research Program of the Chinese Academy of Sciences (XDA17010201). JC and YW acknowledge supports from the National Science Foundation of China (NSFC) through grants 41525015, 41774186, and 41525016.

ORCID iDs

H. Gu https://orcid.org/0000-0002-9831-0618

J. Cui https://orcid.org/0000-0002-4721-8184

P. Lavvas https://orcid.org/0000-0002-5360-3660

References

Adams, N., & Smith, D. 1988, Rate coefficients in Astrochemistry (Dordrecht: Kluwer), 173

Anicich, V. 1993, J. Phys. Chem. Ref. Data, 22, 1469

514 Angelova, G., Novotny, O., Mitchell, J., Rebrion-Rowe, C., et al. 2004, Int. J. Mass Spectrom., 232, 195
515 Baulch, D., Cobos, C., Cox, R., Esser, C., et al. 1992, J. Phys. Chem. Ref. Data, 21, 411
516 Baulch, D., Cobos, C., Cox, R., Frank, P., et al. 1994, J. Phys. Chem. Ref. Data, 23, 847
517 Baulch, D., Bowman, C., Cobos, C., Cox, R., et al. 2005, J. Phys. Chem. Ref. Data, 34, 757
518 Bell, J. M., Bougher, S. W., Waite, Jr. J. H., et al. 2010, J. Geophys. Res., 115, E12018
519 Bell, J. M., Bougher, S. W., Waite, Jr. J. H., et al. 2011, J. Geophys. Res., 116, E11002
520 Brown, R. L., 1973. Int. J. Chem. Kinet., 5, 663
521 Brownsword, R. A., Canosa, A., Rowe, B. R., Sims, I. R., et al. 1997, J. Chem. Phys., 106, 7662
522 Gannon, K., Glowacki, D. , Blitz, M., Hughes, K., Pilling, & M., Seakins, P. 2007, J. Phys. Chem. A, 111,
523 6679
524 Canosa, A., Sims, I. R., Travers, D., Smith, I. W. M., & Rowe, B. R. 1997, AA, 323, 644
525 Carty, D., Le Page, V., Sims, I., & Smith, I. 2001, Chem. Phys. Lett, 344, 310
526 Chang, Y. W., & Wang, N. S. 1994, K. Chem. Phys., 200, 431
527 Clyne, M., & Stedman, D. 1967, J. Phys. Chem., 71, 3071
528 Cravens, T. E., Keller, C. N., & Ray, B. 1997, Planet. Space Sci., 45, 889
529 Cravens, T. E., Robertson, I. P., Clark, J., et al. 2005, Geophys. Res. Lett., 32, L12108
530 Cravens, T. E., Rahmati, A., Fox, J. L., et al. 2017, Journal of Geophysical Research (Space Physics), 122,
531 1102
532 Cui, J., Yelle, R. V., & Volk, K. 2008, J. Geophys. Res., 113, E10004
533 Cui, J., Yelle, R. V., Vuitton, V., et al. 2009a, Icarus, 200, 581
534 Cui, J., Galand, M., Yelle, R. V., et al. 2009b, J. Geophys. Res., 114,A06310
535 Cui, J., Yelle, R. V., Müller-Wodarg, I. C. F., Lavvas,P. P., & Galand, M. 2011, J. Geophys. Res., 116,
536 A11324
537 Cui, J., Yelle, R. V., Strobel, D. F., et al. 2012, J. Geophys. Res., 117, E11006
538 Cui, J., Cao, Y. -T., Lavvas, P. P., et al. 2016, ApJ, 826, L5
539 Cui, J., Wu, X. -S., Gu, H., Jiang, F. -Y., & Wei, Y. 2019, A&A, 621, A23
540 De La Haye, V., Waite, J. H., Cravens, T. E., et al. 2007, Icarus, 191, 236
541 de La Haye, V., Waite, J. H., Cravens, T. E., et al. 2008, Journal of Geophysical Research (Space Physics),
542 113, A11314
543 Dutuit, O., Carrasco, N., Thissen, R., Vuitton, V., et al. 2013, ApJS, 204, #20
544 Edwards, S., Freeman, C., & McEwan, M. 2008, Int. J. Mass Spectrom., 272, 86
545 Ehlerding, A., Hellberg, F., Thomas, R., Kalhori, S., et al. 2004. Phys. Chem. Chem. Phys., 6, 949
546 Ergun, R. E., Morooka, M. W., Andersson, L. A., et al. 2015, Geophys. Res. Lett., 42, 8846
547 Fahr, A., Laufer, A., Klein, R., & Braun, W. 1991, J. Phys. Chem., 95, 3218
548 Fenghour, A., Wakeham, V. A., Vesovic, V., Watson, J. T. R., et al. 1995, J. Phys. Chem. Ref. Data, 24,
549 1649
550 Flynn, L. W., & Thodos, G. 1961, J. Chem. Engineering data, 6, 457
551 Fox, J. L. 1988, Planet. Space Sci., 36, 37
552 Fox, J. L., Galand, M. I., & Johnson, R. E. 2008, Space Sci. Rev., 139, 3
553 Fox, J. L., & Hać, A. B. 2009, Icarus, 204, 524
554 Fox, J. L., & Hać, A. B. 2014, Icarus, 228, 375
555 Fox, J. L., & Hać, A. B. 2018, Icarus, 300, 411
556 Fulle, D., & Hippler, H. 1997, J. Chem. Phys., 106, 8691
557 Geppert, W., Ehlerding, A., Hellberg, F., Kalhori, S., et al. 2004a, Phys. Rev. Lett., 93, #153201.
558 Geppert, W., Thomas, R., Ehlerding, A., Hellberg, F., et al. 2004b, Int. J. Mass Spectrom, 237, 25
559 Goulay, F., Osborn, D., Taatjes, C., Zou, P., Meloni, G., & Leone, S. 2007, Phys. Chem. Chem. Phys., 9,
560 4291
561 Gu. H., Cui. J., Niu., D. -D., et al. 2019, AA, 623, A18

562 Harding, L., Guadagnini, R., Schatz, G., 1993. J. Phys. Chem., 97, 5472
563 Harding, L. B., Georgievskii, Y., & Klippenstein, S. J. 2005, Journal of Physical Chemistry A, 109, 4646
564 Hedelt, P., Ito, Y., Keller, H. U., Reulke, R., et al. 2010, Icarus, 210, 424
565 Herron, J. T. 1999, J. Phys. Chem. Ref. Data, 28, 1453
566 Hess, W. P., Durant Jr., J. L., & Tully, F. P. 1989, J. Phys. Chem., 93, 6402
567 Hoobler, R. J., Opansky, B. J., & Leone, S. R. 1997, J. Phys. Chem. A, 101, 1338
568 Hoobler, R. J., & Leone, S. R., 1997, J. Geophys. Res., 102, 28717
569 Hörst, S. M., Vuitton, V., & Yelle, R. V. 2008, J. Geophys. Res. Planets, 113, E10006
570 Husain, D., & Kirsch, L. J. 1971, Trans. Faraday Soc., 67, 2025
571 Husain, D., & Young, A. N., 1975. J. Chem. Soc. Faraday Trans., 71, 525
572 Janev, R., & Reiter, D. 2004, Phys. Plasmas 11, 780
573 Jamieson, J. W. S., Brown, G. R., & Tanner, J. S. 1970, Can. J. Chem., 48, 3619
574 Jiang, F. -Y., Cui, J., & Xu, J. -Y. 2017, AJ, 154, 271
575 Johnson, R. E., Combi, M. R., Fox, J. L., et al. 2008, Space Sci. Rev., 139, 355
576 Kalhori, S., Viggiano, A., Arnold, S., Rośen, S., et al. 2002. AA, 391, 1159
577 Kamińska, M., Zhaunerchyk, V., Vigren, E., Danielsson, M., et al. 2010, Phys. Rev. A, 81, #062701
578 Keller, C. N., Cravens, T. E., & Gan, L. 1992, J. Geophys. Res., 97, 12117
579 Kerr, J. A., & Parsonage, M. J. 1972, Evaluated Kinetic Data on Gas-phase Addition Reactions (London:
580 Butterworth)
581 Kinsman, A. C., & Roscoe, J. M. 1994, Int. J. Chem. Kinetics, 26, 191
582 Klippenstein, S. J., Harding, L. B., Ruscic, B., Sivaramakrishnan, R., Srinivasan, N. K., Su, M. -C. &
583 Michael, J. V. 2009, J. Phys. Chem. A, 113, 10241
584 Krasnopolsky, V. A. 2014, Icarus, 236, 83
585 Lammer, H., & Bauer, S. J. 1993, Planet. Space Sci., 41, 657
586 Laufer, A. H., Gardner, E. P., Kwok, T. L., & Yung, Y. L. 1983. Icarus, 56, 560
587 Le Padellec, A., Mitchell, J., Al-Khalili, A., Danared, et al. 1999, J. Chem. Phys., 110, 890
588 Larsson, M., Ehlerding, A., Geppert, W., Hellberg, F., et al. 2005, J. Chem. Phys., 122, 156101
589 Lavvas, P. P., Coustenis, A., & Vardavas, I. M. 2008, Planet. Space Sci., 56, 27
590 Lavvas, P. P., Coustenis, A., & Vardavas, I. M. 2008, Planet. Space Sci., 56, 67
591 Laufer, A. H., & Fahr, A. 2004, Chem. Rev., 104, 2813
592 Levine, J. S., McDougal, D. S., Anderson, D. E., et al. 1978, Science, 200, 1048
593 Loison, J.-C., Bergeat, A., Caralp, F., et al. 2006, Journal of Physical Chemistry A, 110, 13500
594 Magee, B. A., Waite, J. H., Mandt, K. E., et al. 2009, Planet. Space Sci., 57, 1895
595 Mandt, K. E., Gell, D. A., Perry, M., et al. 2012, J. Geophys. Res. Planets, 117, E10006
596 Mantei, K. A., & Bair, E. J. 1968, J. Chem. Phys., 49, 3248
597 McEwan, M., & Anicich, V. 2007, Mass Spectrom. Rev. 26, 281
598 McKee, K., Blitz, M. A., Hughes, K. J., et al. 2003, Journal of Physical Chemistry A, 107, 5710
599 McLain, J., Poterya, V., Molek, C., Babcock, L., & Adams, N. 2004, J. Phys. Chem. A, 108, 6704
600 Michael, M., Johnson, R. E., Leblanc, F., et al. 2005, Icarus, 175, 263
601 Michael, M., & Johnson, R. E. 2005, Planet. Space Sci., 53, 1510
602 Mitchell, J., 1990. Phys. Rep., 186, 215
603 Monks, P. S., Nesbitt, F. L., Payne, W. A., Scanlon, M., et al. 1995, J. Phys. Chem., 99, 17151
604 Müller-Wodarg, I. C. F., Yelle, R. V., Cui, J., & Waite, J. H. 2008, J. Geophys. Res., 113, E10005
605 Murphy, J. E., Vakhtin, A. B., & Leone, S R., 2003, Icarus, 163, 175
606 Niemann, H. B., Atreya, S. K., Bauer, S. J., et al. 2005, Nature, 438, 779
607 Nizamov, B., & Leone, S. R. 2004, Journal of Physical Chemistry A, 108, 1746
608 Payne, W. A., Monks, P. S., Nesbitt, F. L., & Stief, L. J. 1996, J. Chem. Phys., 104, 9808
609 Peterson, J., Le Padellec, A., Danared, H., Dunn, G., et al. 1998, J. Chem. Phys., 108, 1978

610 Petrie, S., Chirnside, T., Freeman, C., & McEwan, M. 1991, Int. J. Mass Spectrom, 107, 319
611 Petrie, S., Freeman, C., & McEwan, M. 1992, MNRAS, 257, 438
612 Reisler, H., Mangir, M. S., & Wittig, C., 1980, J. Chem. Phys., 73, 2280
613 Rowley, R. L., Wilding, W. V., Oscarson, J. L., & Yang, Y. 2003, Physical and thermodynamic properties
614 of pure chemicals. Core Edition Plus Supplements, 1
615 Semaniak, J., Larson, Å., Le Padellec, A., Semaniak, J., et al. 1998, ApJ, 498, 886
616 Schaufelberger, A., Wurz, P., Lammer, H., & Kulikov, Y. N. 2012, Planet. Space Sci., 61, 79
617 Sheehan, C., & St.-Maurice, J. P. 2004, J. Geophys. Res., 109, A03302.
618 Shematovich, V. I., Tully, C., & Johnson, R. E. 2001, Adv. Space Sci., 27, 1875
619 Shematovich, V. I., Johnson, R. E., Michael, M., & Luhmann, J. G. 2003, J. Geophys. Res., 108, 5087
620 Sillesen, A., Ratajczak, E., & Pagsberg, P. 1993, Chem. Phys. Lett., 201, 171
621 Sims, I. R., Queffelec, J. L., Travers, D., Rowe, B., et al. 1993, Chem. Phys. Lett., 211, 461
622 Sittler, E. C., Hartle, R. E., Bertucci, C., et al. 2010, Titan from Cassini-huygens, 393
623 Snowden, D., Yelle, R. V., Cui, J., et al. 2013, Icarus, 226, 552
624 Stief, L. J., Nesbitt, F. L., Payne, W. A., Kuo, S. C., et al. 1995, J. Chem. Phys., 102, 5309
625 Stoliarov, S. I., Knyazev, V. D., & Slagle, I. R. 2000, Journal of Physical Chemistry A, 104, 9687
626 Strobel, D. F. 2009, Icarus, 202, 632
627 Strobel, D. F. 2010, Icarus, 208, 878
628 Strobel, D. F. 2012a, Canadian Journal of Physics, 90, 795
629 Strobel, D. F. 2012b, Titan Through Time; Unlocking Titan's Past, Present and Future, 89
630 Strobel, D. F., & Cui, J. 2014, Titan's upper atmosphere/exosphere, escape processes, and rates (Cam-
631 bridge: Cambridge University Press), 355
632 Thomas, R., Hellberg, F., Neau, A., Rośen, S., et al. 2005, Phys. Rev. A, 71, 032711
633 Taylor, H. A., Brinton, H. C., Bauer, S. J., et al. 1980, J. Geophys. Res., 85, 7765
634 Tsang, W., & Hampson, R. F. 1986, J. Phys. Chem. Ref. Data, 15, 1087
635 Tsang, W. 1988, J. Phys. Chem. Ref. Data, 17, 887
636 Tsang, W. 1991, J. Phys. Chem. Ref. Data, 20, 221
637 Tsang, W. 1992, J. Phys. Chem. Ref. Data, 21, 753
638 Tseng, L., & Jones, W. E. 1972, J. Chem. Soc. Faraday Trans., 68, 1267
639 Tucker, O. J., & Johnson, R. E. 2009, Planet. Space Sci., 57, 1889
640 Viggiano, A. A., Ehlerding, A., Arnold, S. T., et al. 2005, Journal of Physics Conference Series, 191
641 Vuitton, V., Doussin, J. F., Bénilan, Y., Raulin, F., & Gazeau, M. C. 2006, Icarus, 185, 287
642 Vuitton, V., Yelle, R. V., & Anicich, V. G. 2006, ApJ, 647, L175
643 Vuitton, V., Yelle, R. V., & McEwan, M. J. 2007, Icarus, 191, 722
644 Vuitton, V., Yelle, R. V., & Cui, J. 2008, J. Geophys. Res., 113, E05007
645 Vuitton, V., Yelle, R. V., Lavvas, P., et al. 2012, ApJ, 744, 11
646 Vuitton, V., Yelle, R. V., Klippenstein, S. J., et al. 2019, Icarus, 324, 120
647 Wagener, R., 1990. Z. Naturforsch. A, 45, 649
648 Wahlund, J. E., Boström, R., Gustafsson, G., et al. 2005, Science, 308, 986
649 Wahlund, J. E., Galand, M., Müller-Wodarg, I., et al. 2009, Planet. Space Sci., 57, 1857
650 Waite, J. H., Niemann, H., Yelle, R. V., et al. 2005, Science, 308, 982
651 Wakelam, V., Herbst, E., Loison, J. C., Smith, I., et al. 2015, ApJS, 199, #21
652 Wallis, M. K. 1978, Planet. Space Sci., 26, 949
653 Wang, H. & Frenklach, M. 1997, J. Chem. Phys., 113, 4146
654 Westlake, J. H., Bell, J. M., Waite, Jr., J. H., et al. 2011, J. Geophys. Res., 116, A03318
655 Wilson, E. H., & Atreya, S. K. 2004, J. Geophys. Res., 109, E06002
656 Xu, Z. -F., Fang, D. -C., Fu, X. -Y., 1998. Int. J. Quantum Chem., 70, 321
657 Yang, D. L., Yu, T., Wang, N. S., et al. 1992, Chemical Physics, 160, 307
658 Yelle, R. V. 1991, ApJ, 383, 380
659 Yelle, R. V., Cui, J., & Müller-Wodarg, I. C. F. 2008, J. Geophys. Res., 113, E10003
660 Zetzsch, C., & Stuhl, F. 1981, Berichte der Bunsengesellschaft für physikalische Chemie, 85, 564
661 Zhu, R. S., Xu, Z. F., & Lin, M. C. 2004, J. Chem. Phys., 120, 6566

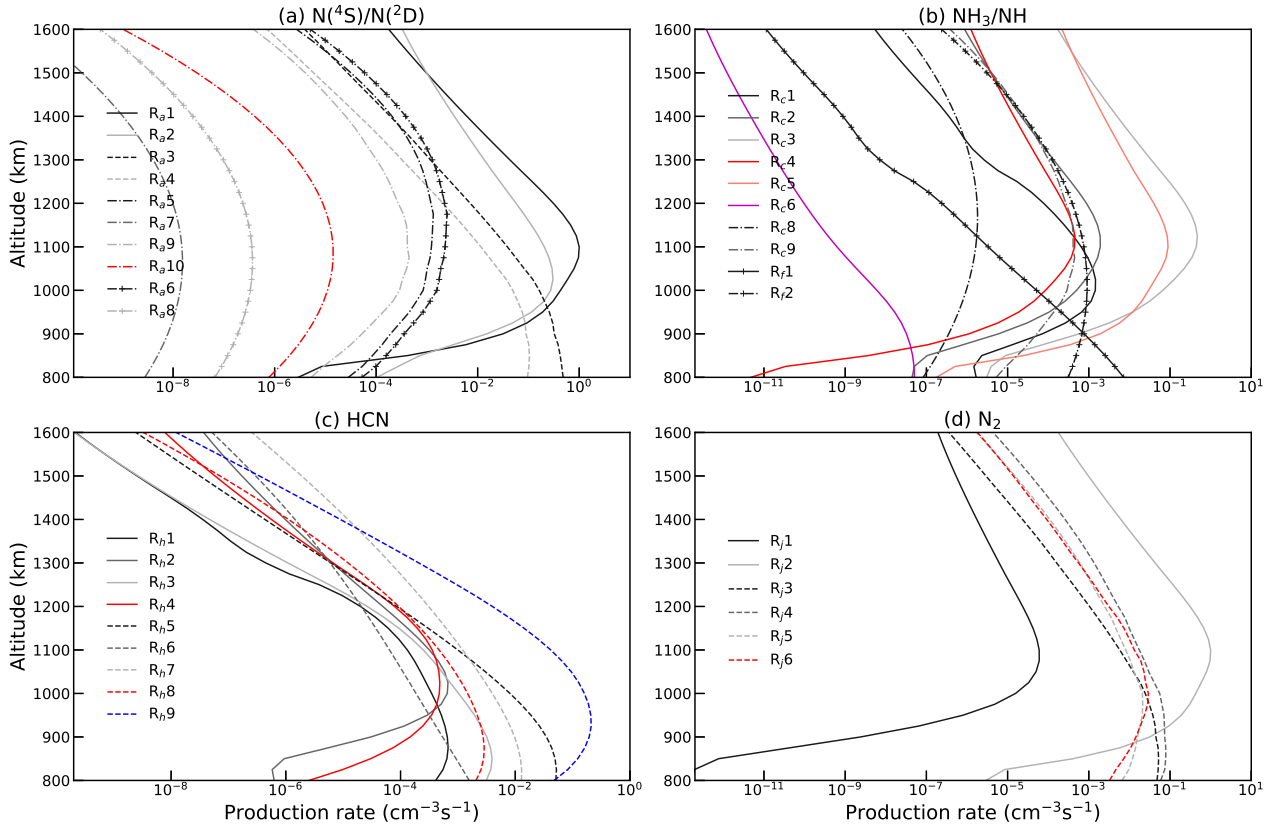

Fig. A.1. The hot neutral production rates calculated via the neutral, ion, and electron density profiles in Figures 1-4, for N(^{4}S) and N(^{2}D) in panel (a), NH_3 and NH in panel (b), HCN in panel (c), as well as N_2 in panel (d), respectively, with the contributions from different chemical channels shown separately. For clarification, the neutral-neutral, ion-neutral, and DR reactions are indicated by the solid, dashed, and dash-dotted lines, respectively.

Appendix A: Supplementary information on the hot neutral production rates and the escape probabilities

For easy reference, we compile in this appendix the detailed information on the hot neutral production rates as well as the escape probabilities used for deriving the C and N escape fluxes. In Table A1, we list all the 146 independent exothermic chemical reactions investigated in the present study, as well as the kinetic energy release, the rate coefficient, the escape flux referred to the surface, the fractional contribution to total N or C escape, and the appropriate references, grouped by species. Note that some reactions are repetitively listed since they are able to produce more than one escaping species. The hot neutral production rates as a function of altitude for all channels are displayed in Figure A1 for N-containing species and in Figure A2 for C-containing species, also grouped by species. These figures provide necessary information on deciding the dominant channel for the production of each species considered here.

Table A.1. Information on the exothermic reactions considered in this study that potentially produce escaping $N(^4S)$, $N(^2D)$, $^3CH_2$, CH_3, NH, CH_4, NH_3, C_2H_2, C_2H_3, HCN, C_2H_4, N_2, C_2H_5, and C_2H_6 in Titan's dayside upper atmosphere. ΔE is the kinetic energy release, k is the reaction coefficient, T_e is the electron temperature, Φ_{esc} is the escape rate of a neutral species via a certain chemical channel, $\Phi_{esc}/\Phi_{esc}^{(tot)}$ is the corresponding fractional contribution to total C or total N escape. When not stated explicitly, all rate coefficients refer to a neutral temperature of 150 K. For three-body reactions, several parameters are provided, which could be used to obtain the appropriate rate coefficients with the aid of Equations 1 and 2 in Section 2.

No.	Reaction	ΔE (eV)	k ($cm^3\ s^{-1}$)	Φ_{esc} (s^{-1})	$\Phi_{esc}/\Phi_{esc}^{(tot)}$	Reference
			$N(^4S)/N(^2D)$			
R_a1/R_j2	$N(^2D) + N_2 \rightarrow N(^4S) + N_2$	1.58	1.70×10^{-14}	6.43×10^{23}	0.708	1
R_a2/R_e7	$NH + CH_3 \rightarrow N(^4S) + CH_4$	0.67	1.00×10^{-11}	1.03×10^{23}	0.113	20
R_a3	$N^+ + CH_4 \rightarrow N(^4S) + CH_4^+$	1.08	5.00×10^{-11}	5.34×10^{21}	5.88×10^{-3}	2, 10
R_a4	$N^+ + HCN \rightarrow N(^4S) + HCN^+$	0.62	2.40×10^{-9}	8.68×10^{20}	9.56×10^{-4}	3
R_a5	$N_2^+ + e \rightarrow N(^4S) + N(^2D)$	1.73	$1.14 \times 10^{-7}(300/T_e)^{0.39}$	2.26×10^{22}	0.025	4, 5
R_a6	$N_2^+ + e \rightarrow 2\ N(^2D)$	0.53	$1.06 \times 10^{-7}(300/T_e)^{0.39}$	5.94×10^{21}	6.54×10^{-4}	4, 5
R_a7	$CN^+ + e \rightarrow N(^4S) + C$	3.39	$1.36 \times 10^{-8}(300/T_e)^{0.55}$	2.71×10^{17}	2.99×10^{-7}	6
R_a8	$CN^+ + e \rightarrow N(^2D) + C$	2.11	$3.26 \times 10^{-7}(300/T_e)^{0.55}$	2.88×10^{18}	3.17×10^{-6}	6
R_a9/R_c8	$N_2H^+ + e \rightarrow N(^4S) + NH$	1.11	$2.47 \times 10^{-7}(300/T_e)^{0.84}$	8.53×10^{20}	9.38×10^{-4}	7
R_a10	$CNC^+ + e \rightarrow N(^4S) + C_2$	2.03	$2.00 \times 10^{-8}(300/T_e)^{0.70}$	7.30×10^{19}	8.04×10^{-5}	7
			$^3CH_2$			
R_b1	$H_2 + C + M \rightarrow {}^3CH_2 + M$	2.26	$k_0 = 2.50 \times 10^{-28}$ $k_\infty = 1.41 \times 10^{-11}$ $k_R = 6.00 \times 10^{-16}$ $F_c = 0.40$	4.60×10^{18}	1.07×10^{-5}	8, 9
R_b2	$N^+ + C_2H_4 \rightarrow {}^3CH_2 + HCNH^+$	4.13	1.58×10^{-10}	6.31×10^{19}	1.47×10^{-4}	10
R_b3	$C_2H_3^+ + e \rightarrow {}^3CH_2 + CH$	0.67	$1.50 \times 10^{-8}(300/T_e)^{0.84}$	4.70×10^{19}	1.10×10^{-4}	11
R_b4	$C_2H_4^+ + e \rightarrow 2\ {}^3CH_2$	1.52	$2.24 \times 10^{-8}(300/T_e)^{0.76}$	2.15×10^{21}	5.02×10^{-3}	12
R_b5/R_d29	$C_2H_5^+ + e \rightarrow {}^3CH_2 + CH_3$	2.02	$2.08 \times 10^{-7}(300/T_e)^{1.20}$	1.51×10^{22}	0.035	13, 14
R_b6/R_e20	$C_2H_6^+ + e \rightarrow {}^3CH_2 + CH_4$	3.98	$4.00 \times 10^{-8}(300/T_e)^{0.70}$	3.55×10^{13}	8.27×10^{-12}	15, 16
R_b7/R_g22	$C_3H_4^+ + e \rightarrow {}^3CH_2 + C_2H_2$	3.89	$1.77 \times 10^{-7}(300/T_e)^{0.67}$	6.51×10^{19}	1.52×10^{-4}	17
R_b8/R_i5	$C_3H_5^+ + e \rightarrow {}^3CH_2 + C_2H_3$	1.90	$3.00 \times 10^{-8}(300/T_e)^{0.70}$	2.75×10^{20}	6.40×10^{-4}	15, 16
R_b9/R_k28	$C_3H_6^+ + e \rightarrow {}^3CH_2 + C_2H_4$	3.64	$1.20 \times 10^{-7}(300/T_e)^{0.70}$	1.05×10^{16}	2.45×10^{-8}	18
R_b10/R_m9	$C_3H_8^+ + e \rightarrow {}^3CH_2 + C_2H_6$	5.46	$1.60 \times 10^{-7}(300/T_e)^{0.70}$	7.76×10^{19}	1.81×10^{-4}	15
			NH			
R_c1	$H + N + M \rightarrow NH + M$	2.26	$k_0 = 5.00 \times 10^{-32}$ $k_\infty = 5.00 \times 10^{-16}$ $k_R = 5.00 \times 10^{-16}$ $F_c = 0.40$	3.19×10^{18}	3.52×10^{-6}	15, 19
R_c2/R_g21	$N(^4S) + C_2H_3 \rightarrow NH + C_2H_2$	1.23	1.31×10^{-11}	1.94×10^{20}	2.13×10^{-4}	10, 21
R_c3/R_k21	$N(^4S) + C_2H_5 \rightarrow NH + C_2H_4$	1.25	7.10×10^{-11}	4.17×10^{22}	0.046	22
R_c4	$N(^2D) + NH_3 \rightarrow NH + NH_2$	0.59	5.00×10^{-11}	1.50×10^{20}	1.65×10^{-4}	1
R_c5/R_d19	$N(^2D) + CH_4 \rightarrow NH + CH_3$	0.69	6.47×10^{-14}	2.77×10^{22}	0.031	1
R_c6	$2\ NH_2 \rightarrow NH + NH_3$	0.38	7.05×10^{-17}	3.71×10^{13}	4.09×10^{-11}	23, 76

To be continued

Table1–continued

No.	Reaction	ΔE (eV)	k ($cm^3\ s^{-1}$)	Φ_{esc} (s^{-1})	$\Phi_{esc}/\Phi_{esc}^{(tot)}$	Reference
R_c7	$NH_2^+ + e \rightarrow NH + H$	0.45	$1.29 \times 10^{-7}(300/T_e)^{0.50}$	3.42×10^{18}	3.76×10^{-6}	24, 25
R_c8/R_a9	$N_2H^+ + e \rightarrow N(^4S) + NH$	1.04	$2.47 \times 10^{-7}(300/T_e)^{0.84}$	1.57×10^{20}	1.73×10^{-4}	7
			CH_3			
R_d1	$H + {}^3CH_2 + M \rightarrow CH_3 + M$	2.98	$k_0 = 2.06 \times 10^{-29}$	4.61×10^{11}	1.08×10^{-12}	27, 28, 29
			$k_\infty = 1.76 \times 10^{-9}$			
R_d2	$H_2 + CH + M \rightarrow CH_3 + M$	2.90	$k_0 = 1.73 \times 10^{-30}$	1.98×10^{18}	4.61×10^{-6}	15, 30
			$k_\infty = 1.13 \times 10^{-10}$			
			$k_R = 6.00 \times 10^{-16}$			
			$F_c = 0.63$			
R_d3/R_k3	$CH + C_2H_6 \rightarrow CH_3 + C_2H_4$	2.30	3.09×10^{-10}	9.04×10^{20}	2.11×10^{-3}	31, 68
R_d4	$CH + C_3H_8 \rightarrow CH_3 + C_3H_6$	2.41	9.21×10^{-11}	8.10×10^{18}	1.89×10^{-6}	32, 70
R_d5	$CH + C_4H_{10} \rightarrow CH_3 + C_4H_8$	2.58	2.89×10^{-10}	7.20×10^{15}	1.68×10^{-9}	32, 70
R_d6/R_g4	$^1CH_2 + C_2H_3 \rightarrow CH_3 + C_2H_2$	3.66	3.00×10^{-11}	3.23×10^{18}	7.53×10^{-6}	37
R_d7/R_k4	$^1CH_2 + C_2H_5 \rightarrow CH_3 + C_2H_4$	2.56	1.50×10^{-11}	5.09×10^{19}	1.19×10^{-4}	37
R_d8	$^1CH_2 + C_2H_6 \rightarrow CH_3 + C_2H_5$	0.50	2.46×10^{-10}	9.25×10^{20}	2.16×10^{-3}	27, 71
R_d9	$^1CH_2 + C_3H_7 \rightarrow CH_3 + C_3H_6$	2.68	1.71×10^{-11}	3.13×10^{14}	7.29×10^{-10}	38
R_d10/R_g6	$^3CH_2 + C_2H_3 \rightarrow CH_3 + C_2H_2$	3.41	3.00×10^{-11}	4.22×10^{19}	9.84×10^{-5}	37
R_d11/R_k7	$^3CH_2 + C_2H_5 \rightarrow CH_3 + C_2H_4$	2.28	3.00×10^{-11}	1.31×10^{21}	3.06×10^{-3}	37
R_d12	$^3CH_2 + C_3H_7 \rightarrow CH_3 + C_3H_6$	2.40	3.00×10^{-12}	6.89×10^{14}	1.61×10^{-9}	38
R_d13	$C_2H + CH_4 \rightarrow CH_3 + C_2H_2$	0.73	4.49×10^{-13}	1.62×10^{21}	3.79×10^{-3}	34
R_d14	$C_2H + C_2H_5 \rightarrow CH_3 + C_3H_3$	1.44	3.00×10^{-11}	2.06×10^{19}	4.81×10^{-5}	37
R_d15	$C_2H + CH_3CCH \rightarrow CH_3 + C_4H_2$	1.06	1.55×10^{-10}	2.57×10^{19}	5.99×10^{-5}	72, 73
R_d16/R_h2	$N(^4S) + C_2H_4 \rightarrow CH_3 + HCN$	1.62	3.18×10^{-16}	9.70×10^{19}	2.26×10^{-4}	35
R_d17	$N(^4S) + C_2H_5 \rightarrow CH_3 + H2CN$	1.34	3.90×10^{-11}	2.37×10^{22}	0.055	22
R_d18	$N(^4S) + CH_3CCH \rightarrow CH_3 + CHCN$	2.25	8.01×10^{-16}	1.89×10^{17}	4.40×10^{-7}	35
R_d19/R_c5	$N(^2D) + CH_4 \rightarrow CH_3 + NH$	0.69	6.47×10^{-14}	2.77×10^{22}	0.065	1
R_d20	$CN + CH_4 \rightarrow CH_3 + HCN$	0.50	6.37×10^{-14}	5.78×10^{19}	1.35×10^{-4}	41, 69
R_d21	$C_2N + CH_4 \rightarrow CH_3 + CHCN$	0.97	6.00×10^{-14}	2.42×10^{19}	5.65×10^{-5}	60
R_d22	$CH_3CN + C_2H \rightarrow CH_3 + HC_3N$	2.09	1.06×10^{-13}	1.64×10^{16}	3.83×10^{-8}	26
R_d23	$C_2H_4^+ + C_2H_4 \rightarrow CH_3 + C_3H_5^+$	0.40	7.03×10^{-10}	4.67×10^{21}	0.011	3
R_d24	$N^+ + CH_4 \rightarrow CH_3 + NH^+$	1.43	5.00×10^{-10}	1.40×10^{22}	0.033	10, 26
R_d25	$HCN^+ + CH_4 \rightarrow CH_3 + HCNH^+$	1.90	1.14×10^{-9}	2.26×10^{22}	0.053	3
R_d26	$CH_4^+ + e \rightarrow CH_3 + H$	0.50	$3.08 \times 10^{-7}(300/T_e)^{0.66}$	1.44×10^{20}	3.37×10^{-4}	25
R_d27	$C_2H_3^+ + e \rightarrow CH_3 + C$	1.19	$3.00 \times 10^{-9}(300/T_e)^{0.84}$	1.33×10^{19}	3.10×10^{-5}	11
R_d28	$C_2H_4^+ + e \rightarrow CH_3 + CH$	0.42	$1.12 \times 10^{-8}(300/T_e)^{0.76}$	2.33×10^{20}	5.45×10^{-5}	12
R_d29/R_b5	$C_2H_5^+ + e \rightarrow CH_3 + {}^3CH_2$	1.89	$2.08 \times 10^{-7}(300/T_e)^{1.20}$	1.43×10^{22}	0.034	13, 14
R_d30	$C_2H_6^+ + e \rightarrow 2\ CH_3$	3.40	$8.00 \times 10^{-8}(300/T_e)^{0.70}$	1.20×10^{13}	2.81×10^{-11}	15, 16
R_d31/R_e21	$C_2H_7^+ + e \rightarrow CH_3 + CH_4$	4.20	$5.00 \times 10^{-7}(300/T_e)^{0.70}$	2.38×10^{20}	5.56×10^{-4}	15
R_d32/R_g23	$C_3H_5^+ + e \rightarrow CH_3 + C_2H_2$	4.43	$3.00 \times 10^{-8}(300/T_e)^{0.70}$	6.41×10^{20}	1.50×10^{-3}	15, 16
R_d33/R_i6	$C_3H_6^+ + e \rightarrow CH_3 + C_2H_3$	3.69	$1.20 \times 10^{-8}(300/T_e)^{0.70}$	1.07×10^{15}	2.50×10^{-9}	18
R_d34/R_k29	$C_3H_7^+ + e \rightarrow CH_3 + C_2H_4$	5.41	$3.80 \times 10^{-8}(300/T_e)^{0.68}$	3.03×10^{20}	7.06×10^{-4}	12
R_d35/R_l7	$C_3H_8^+ + e \rightarrow CH_3 + C_2H_5$	5.31	$1.60 \times 10^{-7}(300/T_e)^{0.70}$	7.46×10^{19}	1.74×10^{-4}	18
R_d36/R_m10	$C_3H_9^+ + e \rightarrow CH_3 + C_2H_6$	5.34	$5.00 \times 10^{-7}(300/T_e)^{0.70}$	3.07×10^{19}	7.17×10^{-5}	15
R_d37/R_f2	$CH_3NH_3^+ + e \rightarrow CH_3 + NH_3$	2.92	$7.00 \times 10^{-7}(300/T_e)^{0.70}$	2.60×10^{20}	6.08×10^{-4}	15, 42
			CH_4			
R_e1	$H + CH_3 + M \rightarrow CH_4 + M$	2.87	$k_0 = 1.62 \times 10^{-28}$	1.36×10^{18}	3.17×10^{-6}	33, 77
			$k_\infty = 2.95 \times 10^{-10}$			
			$k_R = 1.80 \times 10^{-16}$			
			$F_c = 0.56$			

To be continued

Table1–continued

No.	Reaction	ΔE (eV)	k ($cm^3\ s^{-1}$)	Φ_{esc} (s^{-1})	$\Phi_{esc}/\Phi_{esc}^{(tot)}$	Reference
R_e2/R_g7	$CH_3 + C_2H_3 \rightarrow CH_4 + C_2H_2$	1.88	1.95×10^{-10}	3.44×10^{21}	8.03×10^{-3}	45, 78
R_e3/R_k9	$CH_3 + C_2H_5 \rightarrow CH_4 + C_2H_4$	1.92	6.87×10^{-12}	4.88×10^{21}	0.011	15, 26
R_e4	$CH_3 + C_3H_5 \rightarrow CH_4 + CH_2CCH_2$	1.49	1.56×10^{-12}	1.53×10^{20}	3.57×10^{-4}	39
R_e5	$CH_3 + C_3H_6 \rightarrow CH_4 + C_3H_5$	0.53	4.85×10^{-26}	2.86×10^{4}	6.67×10^{-20}	36
R_e6	$CH_3 + C_3H_7 \rightarrow CH_4 + C_3H_6$	2.19	1.00×10^{-11}	3.90×10^{16}	9.11×10^{-8}	15, 38
R_e7/R_a2	$CH_3 + NH \rightarrow CH_4 + N(^4S)$	0.59	1.00×10^{-11}	3.88×10^{22}	0.091	20
R_e8	$CH_3^+ + C_2H_6 \rightarrow CH_4 + C_2H_5^+$	1.22	1.43×10^{-9}	5.35×10^{20}	1.25×10^{-3}	3
R_e9	$CH_4^+ + C_2H_2 \rightarrow CH_4 + C_2H_2^+$	0.67	1.44×10^{-9}	2.04×10^{21}	4.77×10^{-3}	3
R_e10	$CH_4^+ + C_2H_4 \rightarrow CH_4 + C_2H_4^+$	1.28	1.70×10^{-9}	4.17×10^{21}	9.73×10^{-3}	3
R_e11	$CH_5^+ + C_2H_2 \rightarrow CH_4 + C_2H_3^+$	0.57	1.48×10^{-9}	2.50×10^{22}	0.058	3
R_e12	$CH_5^+ + C_2H_4 \rightarrow CH_4 + C_2H_5^+$	0.84	1.50×10^{-9}	3.86×10^{22}	0.090	3
R_e13	$CH_5^+ + HCN \rightarrow CH_4 + HCNH^+$	1.10	5.80×10^{-9}	1.30×10^{23}	0.304	15
R_e14	$C_2H_5^+ + C_2H_2 \rightarrow CH_4 + c\text{-}C_3H_3^+$	0.96	6.84×10^{-11}	1.50×10^{21}	3.51×10^{-3}	3
R_e15	$C_2H_5^+ + C_2H_4 \rightarrow CH_4 + C_3H_5^+$	0.63	3.55×10^{-10}	7.83×10^{21}	0.018	3
R_e16	$N^+ + C_2H_6 \rightarrow CH_4 + HCNH^+$	6.10	1.60×10^{-10}	7.20×10^{18}	1.68×10^{-5}	10
R_e17	$CH_5^+ + e \rightarrow CH_4 + H$	0.49	$5.34 \times 10^{-8}(300/T_e)^{0.72}$	3.11×10^{21}	7.26×10^{-3}	50, 51
R_e18	$C_2H_4^+ + e \rightarrow CH_4 + C$	1.92	$5.60 \times 10^{-7}(300/T_e)^{1.20}$	3.03×10^{20}	7.07×10^{-4}	12
R_e19	$C_2H_5^+ + e \rightarrow CH_4 + CH$	1.79	$1.00 \times 10^{-9}(300/T_e)^{0.76}$	6.73×10^{21}	0.016	13, 14
R_e20/R_b6	$C_2H_6^+ + e \rightarrow CH_4 + {}^3CH_2$	3.48	$4.00 \times 10^{-8}(300/T_e)^{0.70}$	6.17×10^{12}	1.44×10^{-11}	15, 16
R_e21/R_d31	$C_2H_7^+ + e \rightarrow CH_4 + CH_3$	3.94	$5.00 \times 10^{-7}(300/T_e)^{0.70}$	2.25×10^{20}	5.25×10^{-4}	15
R_e22	$C_3H_4^+ + e \rightarrow CH_4 + C_2$	2.28	$1.00 \times 10^{-8}(300/T_e)^{0.67}$	1.97×10^{18}	4.60×10^{-6}	17
R_e23	$C_3H_5^+ + e \rightarrow CH_4 + C_2H$	3.46	$3.00 \times 10^{-8}(300/T_e)^{0.70}$	4.83×10^{20}	1.13×10^{-3}	15, 16
			NH_3			
R_f1	$NH_2 + H + M \rightarrow NH_3 + M$	1.78	$k_0 = 2.52 \times 10^{-28}$ $k_\infty = 2.84 \times 10^{-10}$ $k_R = 2.82 \times 10^{-16}$ $F_c = 0.42$	6.11×10^{15}	6.73×10^{-9}	15, 54, 64
R_f2/R_d37	$CH_3NH_3^+ + e \rightarrow NH_3 + CH_3$	2.58	$7.00 \times 10^{-7}(300/T_e)^{0.70}$	2.25×10^{20}	2.48×10^{-4}	15, 42
			C_2H_2			
R_g1	$H + C_2H + M \rightarrow C_2H_2 + M$	2.99	$k_0 = 9.00 \times 10^{-26}$ $k_\infty = 1.85 \times 10^{-10}$ $k_R = 1.00 \times 10^{-13}$ $F_c = 0.40$	1.66×10^{15}	7.74×10^{-9}	37, 79
R_g2	$H + C_6H_5 \rightarrow C_2H_2 + C_4H_4$	2.03	6.08×10^{-12}	1.65×10^{15}	7.68×10^{-9}	65
R_g3	$^1CH_2 + C_2H \rightarrow C_2H_2 + CH$	1.03	3.00×10^{-11}	3.19×10^{18}	1.49×10^{-5}	37
R_g4/R_d6	$^1CH_2 + C_2H_3 \rightarrow C_2H_2 + CH_3$	2.11	3.00×10^{-11}	1.34×10^{18}	6.27×10^{-6}	37
R_g5	$^3CH_2 + C_2H \rightarrow C_2H_2 + CH$	0.90	3.00×10^{-11}	4.11×10^{19}	1.92×10^{-4}	37
R_g6/R_d10	$^3CH_2 + C_2H_3 \rightarrow C_2H_2 + CH_3$	1.97	3.00×10^{-11}	1.78×10^{19}	8.30×10^{-5}	37
R_g7/R_e2	$CH_3 + C_2H_3 \rightarrow C_2H_2 + CH_4$	1.16	1.95×10^{-10}	1.51×10^{21}	7.09×10^{-3}	45, 78
R_g8	$C_2H + C_2H_3 \rightarrow 2\ C_2H_2$	2.13	1.60×10^{-12}	3.67×10^{16}	1.71×10^{-7}	37
R_g9/R_k10	$C_2H + C_2H_5 \rightarrow C_2H_2 + C_2H_4$	2.19	3.00×10^{-12}	1.40×10^{18}	6.55×10^{-6}	37
R_g10/R_l4	$C_2H + C_2H_6 \rightarrow C_2H_2 + C_2H_5$	0.73	4.15×10^{-11}	1.37×10^{19}	6.37×10^{-5}	34, 52
R_g11	$C_2H + CH_2CCH_2 \rightarrow C_2H_2 + C_3H_3$	1.16	2.58×10^{-10}	2.88×10^{19}	1.34×10^{-4}	60
R_g12	$C_2H + C_3H_5 \rightarrow C_2H_2 + CH_2CCH_2$	2.00	1.20×10^{-11}	8.15×10^{17}	3.80×10^{-6}	39
R_g13	$C_2H + C_3H_7 \rightarrow C_2H_2 + C_3H_6$	2.61	1.00×10^{-11}	2.71×10^{13}	1.27×10^{-11}	38
R_g14	$C_2H + C_3H_8 \rightarrow C_2H_2 + C_3H_7$	0.93	6.10×10^{-11}	5.73×10^{16}	2.67×10^{-7}	34, 52
R_g15	$C_2H + C_4H_10 \rightarrow C_2H_2 + C_4H_9$	0.88	1.15×10^{-10}	1.51×10^{13}	7.07×10^{-11}	53, 75
R_g16/R_k11	$2\ C_2H_3 \rightarrow C_2H_2 + C_2H_4$	1.72	3.50×10^{-11}	9.72×10^{16}	4.53×10^{-7}	66
R_g17/R_m3	$C_2H_3 + C_2H_5 \rightarrow C_2H_2 + C_2H_6$	1.76	8.00×10^{-13}	8.96×10^{16}	4.18×10^{-7}	37

To be continued

Table1–continued

No.	Reaction	ΔE (eV)	k ($cm^3\ s^{-1}$)	Φ_{esc} (s^{-1})	$\Phi_{esc}/\Phi_{esc}^{(tot)}$	Reference
R_g18	$C_2H_3 + C_3H_3 \rightarrow C_2H_2 + CH_3CCH$	1.44	8.00×10^{-12}	3.09×10^{16}	1.44×10^{-7}	27, 44
R_g19	$C_2H_3 + C_3H_5 \rightarrow C_2H_2 + C_3H_6$	1.43	8.00×10^{-12}	1.17×10^{17}	5.44×10^{-7}	39
R_g20	$C_2H_3 + C_3H_7 \rightarrow C_2H_2 + C_3H_8$	1.73	2.00×10^{-12}	1.03×10^{12}	4.79×10^{-12}	38
R_g21/R_c2	$N(^4S) + C_2H_3 \rightarrow C_2H_2 + NH$	0.71	1.31×10^{-11}	7.88×10^{19}	3.68×10^{-4}	10, 21
R_g22/R_b7	$C_3H_4^+ + e \rightarrow C_2H_2 + {}^3CH_2$	2.09	$1.77 \times 10^{-7}(300/T_e)^{0.67}$	1.37×10^{19}	6.40×10^{-5}	17
R_g23/R_d32	$C_3H_5^+ + e \rightarrow C_2H_2 + CH_3$	2.56	$3.00 \times 10^{-8}(300/T_e)^{0.70}$	1.71×10^{20}	8.00×10^{-4}	15, 16
			HCN			
R_h1	$H + CN + M \rightarrow HCN + M$	2.74	$k_0 = 8.78 \times 10^{-31}$ $k_\infty = 2.44 \times 10^{-10}$ $k_R = 1.00 \times 10^{-13}$ $F_c = 0.40$	3.94×10^{16}	$4.33 \times 10^{-8}/9.19 \times 10^{-8}$	40
R_h2/R_d16	$N(^4S) + C_2H_4 \rightarrow HCN + CH_3$	0.90	3.18×10^{-16}	1.62×10^{18}	$1.78 \times 10^{-6}/3.78 \times 10^{-5}$	35
R_h3	$CN + C_3H_8 \rightarrow HCN + C_3H_7$	0.67	1.18×10^{-10}	9.91×10^{15}	$1.09 \times 10^{-8}/2.31 \times 10^{-9}$	46, 74
R_h4	$CN + CH_2NH \rightarrow HCN + H_2CN$	0.76	2.80×10^{-11}	3.30×10^{17}	$3.62 \times 10^{-7}/7.70 \times 10^{-7}$	55, 75
R_h5	$CH_3^+ + HC_3N \rightarrow HCN + c\text{-}C_3H_3^+$	1.45	1.43×10^{-9}	2.53×10^{17}	$2.79 \times 10^{-7}/5.91 \times 10^{-7}$	3
R_h6	$CN^+ + CH_4 \rightarrow HCN + CH_3^+$	1.83	5.00×10^{-10}	3.51×10^{18}	$3.86 \times 10^{-6}/8.19 \times 10^{-6}$	3
R_h7	$HCN^+ + C_2H_2 \rightarrow HCN + C_2H_2^+$	1.07	1.15×10^{-9}	1.37×10^{19}	$1.51 \times 10^{-5}/3.20 \times 10^{-5}$	3
R_h8	$CNC^+ + C_2H_4 \rightarrow HCN + c\text{-}C_3H_3^+$	2.86	1.95×10^{-10}	1.07×10^{18}	$1.18 \times 10^{-6}/2.50 \times 10^{-6}$	43
R_h9	$HCNH^+ + C_3H_3N \rightarrow HCN + C_3H_4N^+$	1.14	4.50×10^{-9}	2.02×10^{18}	$2.22 \times 10^{-6}/4.70 \times 10^{-6}$	56, 57
			C_2H_3			
R_i1	$H + C_2H_2 + M \rightarrow C_2H_3 + M$	0.77	$k_0 = 5.88 \times 10^{-30}$ $k_\infty = 3.74 \times 10^{-15}$ $k_R = 2.16 \times 10^{-18}$ $F_c = 0.18$	3.79×10^{13}	1.77×10^{-10}	32, 77
R_i2/R_k5	$^1CH_2 + C_3H_5 \rightarrow C_2H_3 + C_2H_4$	1.25	6.67×10^{-11}	1.34×10^{19}	6.07×10^{-5}	39
R_i3	$C_2H_3CN + C_2 \rightarrow C_2H_3 + C_3N$	1.62	4.4×10^{-10}	3.53×10^{15}	1.65×10^{-8}	49, 59
R_i4	$C_3H_4^+ + e \rightarrow C_2H_3 + CH$	2.09	$2.95 \times 10^{-8}(300/T_e)^{0.67}$	4.51×10^{18}	2.10×10^{-5}	17
R_i5/R_b8	$C_3H_5^+ + e \rightarrow C_2H_3 + {}^3CH_2$	0.99	$3.00 \times 10^{-8}(300/T_e)^{0.70}$	8.31×10^{19}	3.37×10^{-4}	15, 16
R_i6/R_d33	$C_3H_6^+ + e \rightarrow C_2H_3 + CH_3$	2.05	$1.20 \times 10^{-8}(300/T_e)^{0.70}$	4.70×10^{14}	1.92×10^{-8}	18
R_i7/R_m11	$C_4H_9^+ + e \rightarrow C_2H_3 + C_2H_6$	3.69	$8.70 \times 10^{-9}(300/T_e)^{0.59}$	8.15×10^{18}	3.81×10^{-5}	18, 48
			N_2			
R_j1	$2\ N(^4S) + M \rightarrow N_2 + M$	4.91	$k_0 = 4.46 \times 10^{-32}$ $k_\infty = 5.00 \times 10^{-16}$ $k_R = 5.00 \times 10^{-16}$ $F_c = 0.40$	4.63×10^{19}	1.02×10^{-4}	58
R_j2/R_a1	$N(^2D) + N_2 \rightarrow N_2 + N(^4S)$	0.79	1.70×10^{-14}	2.53×10^{22}	0.056	1
R_j3	$N^+ + HCN \rightarrow N_2 + CH^+$	1.28	1.29×10^{-9}	1.11×10^{20}	2.43×10^{-4}	3
R_j4	$N_2^+ + C_2H_2 \rightarrow N_2 + C_2H_2^+$	2.02	9.40×10^{-10}	1.93×10^{21}	4.26×10^{-3}	10
R_j5	$N_2^+ + HCN \rightarrow N_2 + HCN^+$	0.99	3.90×10^{-10}	4.31×10^{20}	9.48×10^{-4}	3
R_j6	$N_2H^+ + HCN \rightarrow N_2 + HCNH^+$	1.16	3.20×10^{-9}	4.48×10^{20}	9.86×10^{-4}	3
			C_2H_4			
R_k1	$H + C_2H_3 + M \rightarrow C_2H_4 + M$	2.40	$k_0 = 8.54 \times 10^{-27}$ $k_\infty = 1.76 \times 10^{-10}$	1.51×10^{12}	7.08×10^{-12}	47
R_k2	$C + CH_4 + M \rightarrow C_2H_4 + M$	3.06	2.00×10^{-15}	4.37×10^{19}	2.04×10^{-4}	67
R_k3/R_d3	$CH + C_2H_6 \rightarrow C_2H_4 + CH_3$	1.23	3.09×10^{-10}	4.13×10^{20}	1.93×10^{-3}	31, 68
R_k4/R_d7	$^1CH_2 + C_2H_5 \rightarrow C_2H_4 + CH_3$	1.37	1.50×10^{-11}	2.41×10^{19}	1.13×10^{-4}	37
R_k5/R_i2	$^1CH_2 + C_3H_5 \rightarrow C_2H_4 + C_2H_3$	1.21	6.67×10^{-11}	1.30×10^{19}	6.26×10^{-5}	39
R_k6/R_l2	$^1CH_2 + C_3H_7 \rightarrow C_2H_4 + C_2H_5$	1.82	4.29×10^{-11}	4.26×10^{14}	1.99×10^{-9}	38

To be continued

Table1–continued

No.	Reaction	ΔE (eV)	k ($cm^3\ s^{-1}$)	Φ_{esc} (s^{-1})	$\Phi_{esc}/\Phi_{esc}^{(tot)}$	Reference
R_k7/R_d11	$^3CH_2 + C_2H_5 \rightarrow C_2H_4 + CH_3$	1.22	3.00×10^{-11}	5.99×10^{20}	2.79×10^{-3}	37
R_k8/R_l3	$^3CH_2 + C_3H_7 \rightarrow C_2H_4 + C_2H_5$	1.62	3.00×10^{-12}	3.48×10^{14}	1.62×10^{-9}	38
R_k9/R_e3	$CH_3 + C_2H_5 \rightarrow C_2H_4 + CH_4$	1.10	6.87×10^{-12}	2.27×10^{21}	0.011	15, 26
R_k10/R_g9	$C_2H + C_2H_5 \rightarrow C_2H_4 + C_2H_2$	2.03	3.00×10^{-12}	2.09×10^{18}	9.74×10^{-6}	37
R_k11/R_g16	$C_2H_3 + C_2H_3 \rightarrow C_2H_4 + C_2H_2$	1.60	3.50×10^{-11}	1.27×10^{17}	5.91×10^{-7}	66
R_k12	$C_2H_3 + C_2H_5 \rightarrow 2\ C_2H_4$	1.64	1.50×10^{-11}	2.40×10^{17}	2.10×10^{-5}	66
R_k13	$C_2H_3 + C_3H_5 \rightarrow C_2H_4 + CH_2CCH_2$	1.39	4.00×10^{-12}	8.05×10^{16}	3.76×10^{-7}	39
R_k14	$C_2H_3 + C_3H_7 \rightarrow C_2H_4 + C_3H_6$	1.97	2.00×10^{-12}	2.31×10^{12}	1.08×10^{-11}	38
R_k15	$C_2H_3 + C_4H_3 \rightarrow C_2H_4 + C_4H_2$	2.07	1.75×10^{-12}	1.15×10^{15}	5.38×10^{-9}	27
R_k16/R_m4	$2\ C_2H_5 \rightarrow C_2H_4 + C_2H_6$	1.44	2.40×10^{-12}	1.24×10^{19}	5.81×10^{-5}	33
R_k17	$C_2H_5 + C_3H_3 \rightarrow C_2H_4 + CH_3CCH$	1.37	6.68×10^{-12}	1.39×10^{18}	6.48×10^{-6}	37, 44
R_k18	$C_2H_5 + C_3H_5 \rightarrow C_2H_4 + C_3H_6$	1.36	6.68×10^{-12}	5.27×10^{18}	2.46×10^{-5}	34
R_k19	$C_2H_5 + C_3H_7 \rightarrow C_2H_4 + C_3H_8$	1.67	5.00×10^{-11}	6.37×10^{13}	7.82×10^{-9}	15, 38
R_k20	$C_2H_5 + C_4H_3 \rightarrow C_2H_4 + C_4H_4$	2.13	8.00×10^{-13}	4.50×10^{8}	2.10×10^{-15}	27
R_k21/R_c3	$N(^4S) + C_2H_5 \rightarrow C_2H_4 + NH$	0.67	7.10×10^{-11}	1.87×10^{15}	8.73×10^{-9}	22
R_k22	$C_2H_5^+ + NH_3 \rightarrow C_2H_4 + NH_4^+$	0.89	2.09×10^{-9}	4.22×10^{19}	1.97×10^{-4}	43
R_k23	$C_2H_5^+ + CH_2NH \rightarrow C_2H_4 + CH_2NH_2^+$	1.03	2.57×10^{-9}	5.40×10^{20}	2.52×10^{-3}	61
R_k24	$C_2H_5^+ + CH_3CN \rightarrow C_2H_4 + CH_4CN^+$	1.58	3.80×10^{-9}	3.64×10^{20}	1.70×10^{-3}	3
R_k25	$C_2H_5^+ + HC_3N \rightarrow C_2H_4 + HC_3NH^+$	0.75	3.55×10^{-9}	7.39×10^{18}	3.45×10^{-5}	3
R_k26	$C_2H_5^+ + C_3H_3N \rightarrow C_2H_4 + C_3H_3NH^+$	1.51	5.80×10^{-9}	2.35×10^{19}	1.10×10^{-4}	15
R_k27	$C_2H_5^+ + C_3H_5N \rightarrow C_2H_4 + C_3H_5NH^+$	1.10	6.00×10^{-9}	2.10×10^{16}	9.81×10^{-8}	15
R_k28/R_b9	$C_3H_6^+ + e \rightarrow C_2H_4 + {}^3CH_2$	1.82	$1.20 \times 10^{-7}(300/T_e)^{0.70}$	3.81×10^{15}	1.78×10^{-8}	18
R_k29/R_d34	$C_3H_7^+ + e \rightarrow C_2H_4 + CH_3$	2.90	$3.80 \times 10^{-8}(300/T_e)^{0.68}$	1.56×10^{20}	7.27×10^{-4}	12
			C_2H_5			
R_l1	$H + C_2H_4 + M \rightarrow C_2H_5 + M$	0.77	$k_0 = 1.64 \times 10^{-28}$ $k_\infty = 4.85 \times 10^{-14}$ $k_R = 5.62 \times 10^{-17}$ $F_c = 0.20$	2.85×10^{16}	1.33×10^{-7}	34, 77
R_l2/R_k6	$^1CH_2 + C_3H_7 \rightarrow C_2H_5 + C_2H_4$	1.76	4.29×10^{-11}	2.40×10^{14}	1.12×10^{-9}	38
R_l3/R_k8	$^3CH_2 + C_3H_7 \rightarrow C_2H_5 + C_2H_4$	1.56	3.00×10^{-12}	2.00×10^{14}	9.33×10^{-10}	38
R_l4/R_g11	$C_2H + C_2H_6 \rightarrow C_2H_2 + C_2H_5$	0.65	4.15×10^{-11}	1.68×10^{19}	1.51×10^{-6}	52
R_l5	$C_2H + C_3H_7 \rightarrow C_2H_5 + C_3H_3$	1.22	2.00×10^{-11}	2.00×10^{13}	9.32×10^{-11}	38
R_l6	$C_3H_6^+ + e \rightarrow C_2H_5 + CH$	0.91	$8.00 \times 10^{-8}(300/T_e)^{0.70}$	3.34×10^{18}	1.56×10^{-5}	18
R_l7/R_d35	$C_3H_8^+ + e \rightarrow C_2H_5 + CH_3$	2.75	$1.60 \times 10^{-7}(300/T_e)^{0.70}$	1.58×10^{19}	7.38×10^{-5}	18
			C_2H_6			
R_m1	$H + C_2H_5 + M \rightarrow C_2H_6 + M$	2.09	$k_0 = 2.38 \times 10^{-30}$ $k_\infty = 1.66 \times 10^{-10}$	4.57×10^{9}	2.13×10^{-14}	62, 63
R_m2	$2\ CH_3 + M \rightarrow C_2H_6 + M$	1.85	$k_0 = 2.04 \times 10^{-25}$ $k_\infty = 7.45 \times 10^{-11}$ $k_R = 1.65 \times 10^{-13}$ $F_c = 0.37$	6.18×10^{21}	0.029	15
R_m3/R_g17	$C_2H_3 + C_2H_5 \rightarrow C_2H_6 + C_2H_2$	1.53	8.00×10^{-13}	6.76×10^{16}	3.16×10^{-7}	37
R_m4/R_k16	$2\ C_2H_5 \rightarrow C_2H_6 + C_2H_4$	1.34	2.40×10^{-12}	7.08×10^{18}	3.30×10^{-5}	33
R_m5	$C_2H_5 + C_3H_7 \rightarrow C_2H_6 + C_3H_6$	1.72	5.00×10^{-11}	4.51×10^{13}	2.10×10^{-10}	15, 38
R_m6	$C_2H_5 + C_4H_3 \rightarrow C_2H_6 + C_4H_2$	1.74	8.00×10^{-13}	7.07×10^{15}	3.30×10^{-8}	27
R_m7	$C_2H_3^+ + C_3H_8 \rightarrow C_2H_6 + C_3H_5^+$	0.82	5.00×10^{-11}	3.02×10^{15}	1.41×10^{-8}	26
R_m8	$C_3H_7^+ + e \rightarrow C_2H_6 + CH$	1.17	$3.80 \times 10^{-7}(300/T_e)^{0.68}$	2.25×10^{20}	1.05×10^{-3}	20
R_m9/R_b10	$C_3H_8^+ + e \rightarrow C_2H_6 + {}^3CH_2$	2.55	$1.60 \times 10^{-7}(300/T_e)^{0.70}$	6.65×10^{18}	3.10×10^{-5}	15
R_m10/R_d36	$C_3H_9^+ + e \rightarrow C_2H_6 + CH_3$	2.67	$5.00 \times 10^{-7}(300/T_e)^{0.70}$	8.19×10^{18}	3.82×10^{-5}	15

To be continued

Table1–continued

No.	Reaction	ΔE (eV)	k ($cm^3\ s^{-1}$)	Φ_{esc} (s^{-1})	$\Phi_{esc}/\Phi_{esc}^{(tot)}$	Reference
R_m11/R_i7	$C_4H_9^+ + e \rightarrow C_2H_6 + C_2H_3$	3.32	$8.70 \times 10^{-9}(300/T_e)^{0.59}$	2.20×10^{18}	1.03×10^{-5}	18, 48

[1]Herron (1999), [2]Cravens et al. (1997), [3]McEwan & Anicich (2007), [4]Sheehan & St.-Maurice (2004), [5]Peterson et al. (1998), [6]Le Padellec et al. (1999), [7]Wakelam et al. (2015), [8]Husain & Young (1975), [9]Harding et al. (1993), [10]Dutuit et al. (2013), [11]Kalhori et al. (2002), [12]Ehlerding et al. (2004), [13]McLain et al. (2004), [14]Geppert et al. (2004a), [15]Vuitton et al. (2019), [16]Janev & Reiter (2004), [17]Geppert et al. (2004b), [18]Angelova et al. (2004), [19]Brown (1973), [20]De La Haye et al. (2007), [21]Payne et al. (1996), [22]Stief et al. (1995), [23]Xu et al. (1998), [24]Mitchell (1990), [25]Thomas et al. (2005), [26]Zhu et al. (2004), [27]Lavvas et al (2008a), [28]Laufer et al. (1983), [29]Fulle & Hippler (1997), [30]Brownsword et al. (1997), [31]Canosa et al. (1997), [32]Baulch et al. (1992), [33]Baulch et al. (1994), [34]Baulch et al. (2005), [35]Kerr & Parsonage (1972), [36]Kinsman & Roscoe (1994), [37]Tsang & Hampson (1986), [38]Tsang (1988), [39]Tsang (1991), [40]Tsang (1992), [41]Sims et al. (1993), [42]Adams & Smith (1988), [43]Anicich (1993), [44]Vuitton et al. (2006a), [45]Fahr et al. (1991), [46]Hess et al. (1989), [47]Monks et al. (1995), [48]Larsson et al. (2005), [49]Jamieson et al. (1970), [50]kamińska et al. (2010), [51]Semaniak et al. (1998), [52]Murphy et al. (2003), [53]Hoobler et al. (1997), [54]Zetzsch & Stuhl (1981), [55]Chang & Wang (1994), [56]Petrie et al. (1991), [57]Petrie et al. (1992), [58]Clyne & Stedman (1967), [59]Reisler et al. (1980), [60]Hoobler & Leone (1997), [61]Edwards et al. (2008), [62]Tseng & Jones (1972), [63]Sillesen et al. (1993), [64]Mantei & Bair (1968), [65]Wang & Frenklach (1997), [66]Laufer & Fahr (2004), [67]Husain & Kirsch (1971), [68]McKee et al. (2003), [69]Cannon et al. (2007), [70]Loison et al. (2006), [71]Wagener (1990), [72]Carty et al. (2001), [73]Goulay et al. (2007), [74]Yang et al. (1992), [75]Nizamov & Leone (2004), [76]Klippenstein et al. (2009), [77]Vuitton et al. (2012), [78]Stoliarov et al. (2000), [79]Harding et al. (2005).

In Table A2, we list the parameters (a_1, a_2, and a_3) used to describe the altitude dependence of escape probability for each species and for a range of selected nascent energy according to Equation 34 in Section 3. For an arbitrary nascent energy within the prescribed range, the escape probability profile could be determined with the aid of Equation 35 using a set of parameters (b_1, b_2, b_3, and b_4). These parameters are listed in Table A3 for reference.

Table A.2. Best-fit parameters (a_1, a_2, and a_3) to describe the altitude dependence of escape probability for a given species at a given nascent energy (see Equation 34 for details).

Species		Energy (eV)							a_2
		0.5	1.0	1.5	2.5	3.5	5.0	6.5	
$N(^4S)/N(^2D)$	a_1	0.272	0.274	0.275	0.276	0.276	0.277	0.277	1450
	a_3	0.180	0.234	0.267	0.303	0.326	0.347	0.361	
$^3CH_2/CH_3/CH_4$	a_1	0.236	0.268	0.281	0.297	0.306	0.316	0.319	1500
	a_3	0.135	0.181	0.206	0.235	0.254	0.271	0.283	
NH/NH_3	a_1	0.233	0.265	0.280	0.297	0.307	0.315	0.318	1500
	a_3	0.130	0.177	0.202	0.231	0.250	0.268	0.279	
		Energy (eV)							
		1	1.5	2.0	3.0	4.0	5.0	–	
C_2H_2	a_1	0.235	0.252	0.263	0.279	0.289	0.296	–	1530
	a_3	0.157	0.182	0.199	0.224	0.239	0.251	–	
HCN	a_1	0.197	0.221	0.237	0.257	0.269	0.279	–	1600
	a_3	0.151	0.178	0.196	0.221	0.236	0.249	–	
N_2	a_1	0.244	0.256	0.263	0.274	0.282	0.285	–	1520
	a_3	0.178	0.206	0.226	0.253	0.270	0.283	–	
C_2H_3/C_2H_4	a_1	0.230	0.247	0.258	0.273	0.282	0.290	–	1540
	a_3	0.164	0.191	0.208	0.234	0.251	0.263	–	
C_2H_5/C_2H_6	a_1	0.219	0.240	0.252	0.266	0.277	0.285	–	1560
	a_3	0.151	0.178	0.196	0.221	0.236	0.249	–	

Table A.3. Best-fit parameters (b_1, b_2, b_3, and b_4) to describe the energy dependences of the parameters listed in Table A2 (a_1, a_2, and a_3) (see Equation 35 for details).

Species	b_1	b_2	b_3	b_4
$N(^4S)/N(^2D)$	−0.0073	0.277	0.0709	0.234
$^3CH_2/CH_3/CH_4$	−0.129	0.313	0.0575	0.179
NH/NH_3	−0.134	0.313	0.0579	0.175
C_2H_2	0.0383	0.236	0.0587	0.158
HCN	0.0506	0.199	0.0608	0.153
N_2	0.0368	0.232	0.0619	0.165
C_2H_3/C_2H_4	0.0259	0.245	0.0657	0.179
C_2H_5/C_2H_6	0.0399	0.222	0.0646	0.167

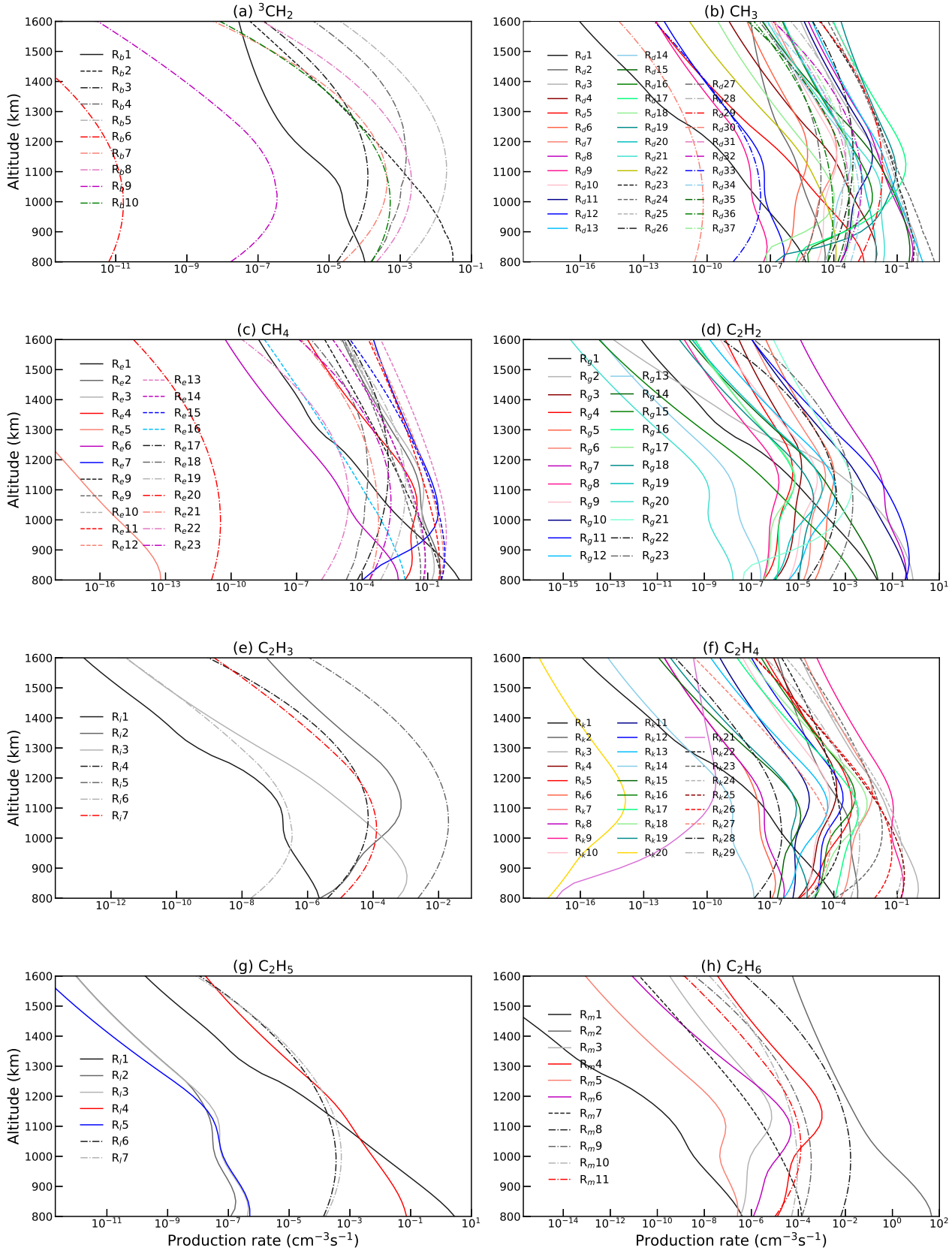

Fig. A.2. Similar to Figure A1 but for $^3CH_2$ in panel (a), CH_3 in panel (b), CH_4 in panel (c), C_2H_2 in panel (d), C_2H_3 in panel (e), C_2H_4 in panel (f), C_2H_5 in panel (g), and C_2H_6 in panel (h), respectively.